Original article

MOLECULAR METABOLISM

# TNP [N2-(m-Trifluorobenzyl), N6-(p-nitrobenzyl) purine] ameliorates diet induced obesity and insulin resistance *via* inhibition of the IP6K1 pathway

**Sarbani Ghoshal [1], Qingzhang Zhu [1], Alice Asteian [2,5], Hua Lin [2], Haifei Xu [3], Glen Ernst [4], James C. Barrow [4], Baoji Xu [3], Michael D. Cameron [2], Theodore M. Kamenecka [2], Anutosh Chakraborty [1,*]**

## ABSTRACT

**Objective:** Obesity and type 2 diabetes (T2D) lead to various life-threatening diseases such as coronary heart disease, stroke, osteoarthritis, asthma, and neurodegeneration. Therefore, extensive research is ongoing to identify novel pathways that can be targeted in obesity/T2D. Deletion of the inositol pyrophosphate (5-IP7) biosynthetic enzyme, inositol hexakisphosphate kinase-1 (IP6K1), protects mice from high fat diet (HFD) induced obesity (DIO) and insulin resistance. Yet, whether this pathway is a valid pharmacologic target in obesity/T2D is not known. Here, we demonstrate that TNP [N2-(m-Trifluorobenzyl), N6-(p-nitrobenzyl)purine], a pan-IP6K inhibitor, has strong anti-obesity and anti-diabetic effects in DIO mice.

**Methods:** Q-NMR, GTT, ITT, food intake, energy expenditure, QRT-PCR, ELISA, histology, and immunoblot studies were conducted in short (2.5-week)- and long (10-week)-term TNP treated DIO C57/BL6 WT and IP6K1-KO mice, under various diet and temperature conditions.

**Results:** TNP, when injected at the onset of HFD-feeding, decelerates initiation of DIO and insulin resistance. Moreover, TNP facilitates weight loss and restores metabolic parameters, when given to DIO mice. However, TNP does not reduce weight gain in HFD-fed IP6K1-KO mice. TNP specifically enhances insulin sensitivity in DIO mice via Akt activation. TNP decelerates weight gain primarily by enhancing thermogenic energy expenditure in the adipose tissue. Accordingly, TNP's effect on body weight is partly abolished whereas its impact on glucose homeostasis is preserved at thermoneutral temperature.

**Conclusion:** Pharmacologic inhibition of the inositol pyrophosphate pathway has strong therapeutic potential in obesity, T2D, and other metabolic diseases.

© 2016 The Author(s). Published by Elsevier GmbH. This is an open access article under the CC BY-NC-ND license (http://creativecommons.org/licenses/by-nc-nd/4.0/).

**Keywords** IP6K; Inositol pyrophosphate; Obesity; Energy expenditure; Diabetes; Akt

## 1. INTRODUCTION

In the US, 34.9% of adults are obese of which 9.3% have diabetes. Obesity, especially when combined with type-2 diabetes (T2D), leads to several co-morbid conditions such as coronary heart disease, stroke, hypercholesterolemia, fatty liver, sleep apnea, osteoarthritis, and various other diseases. Obesity promotes insulin resistance [1,2]. Therefore, a drug that reduces fat mass and enhances insulin sensitivity is expected to ameliorate obesity and T2D, when applied in combination with lifestyle intervention [3–8]. Unfortunately, current

[1]Department of Metabolism and Aging, The Scripps Research Institute, Jupiter, FL 33458, USA [2]Department of Molecular Therapeutics, The Scripps Research Institute, Jupiter, FL 33458, USA [3]Department of Neuroscience, The Scripps Research Institute, Jupiter, FL 33458, USA [4]Drug Discovery Division, Lieber Institute for Brain Development, Baltimore, MD 21205, USA

[5] Current address: Department of Chemistry, University of Cambridge, UK.

*Corresponding author. Fax: +1 561 228 3059. E-mail: achakrab@scripps.edu (A. Chakraborty).

*Abbreviations:* IP6K, Inositol hexakisphosphate kinase; 5-IP7, diphosphoinositol pentakisphosphate; TNP, [N2-(m-Trifluorobenzyl), N6-(p-nitrobenzyl)purine]; CD, chow-diet; HFD, high-fat diet; DIO, diet-induced obesity; T2D, type-2 diabetes; EE, energy expenditure; H&E, hematoxylin and eosin; AUC, area under curve; WAT, white adipose tissue; EWAT, epididymal adipose tissue; IWAT, inguinal adipose tissue; RWAT, retroperitoneal adipose tissue; BAT, brown adipose tissue; Q-NMR, quantitative nuclear magnetic resonance; HPLC, high performance liquid chromatography; PCR, polymerase chain reaction; QRT-PCR, quantitative reverse transcription polymerase chain reaction; GTT, glucose tolerance test; ITT, insulin tolerance test; T308, threonine 308; S473, serine 473; S9, serine 9; $VO_2$, volume of oxygen consumption; RER, Respiratory exchange ratio; ALT, alanine aminotransferase; AST, aspartate transaminase; IP6K1-KO, IP6K1 knockout; GSK3, glycogen synthase kinase; PKA, protein kinase A; UCP-1/3, uncoupling protein 1/3; Cidea, cell death activator-A; PPAR$\gamma$, peroxisome proliferator-activated receptor gamma; PGC1$\alpha$, PPAR coactivator 1 alpha; PRDM16, PR domain containing 16; CPT1a, carnitine palmitoyltransferase I; SREV-TNP, short-term TNP treatment for reversal of DIO; Pro-TNP, TNP treatment for protection against DIO; Rev-TNP, long-term TNP treatment for reversal of DIO; RevT-TNP, Long-term TNP treatment for reversal of DIO at thermoneutral temperature

Received July 22, 2016 • Revision received August 10, 2016 • Accepted August 15, 2016 • Available online 21 August 2016

http://dx.doi.org/10.1016/j.molmet.2016.08.008

 © 2016 The Author(s). Published by Elsevier GmbH. This is an open access article under the CC BY-NC-ND license (http://creativecommons.org/licenses/by-nc-nd/4.0/). 

anti-obesity and anti-diabetic medications are only partly effective [3,6,9]; thus, a safe and effective drug has a projected market of $3.7 billion [5]. Therefore, extensive research is ongoing to identify targetable proteins to develop pharmacotherapy against obesity and T2D [10–14]. A majority of the studies are conducted in diet induced obese (DIO) rodents, which resemble human polygenic obesity [15]. The C57BL6 mouse is a particularly good DIO model, which mimics human metabolic aberrations that are observed in obesity [16,17]. Moreover, enzymes, especially kinases, are considered attractive drug targets due to their catalytic specificity [11,18].

Inositol pyrophosphates regulate diverse cellular processes [19–23]. The most characterized inositol pyrophosphate in mammals, is 5-IP7, which is synthesized by a family of three inositol hexakisphosphate kinase enzymes, of which IP6K1 is the major isoform [19,24,25]. At lower ATP/ADP ratio, IP6Ks dephosphorylate IP6 to IP5* [I(2, 3, 4, 5, 6) P5 [26]. IP6Ks regulate cellular targets by diverse mechanisms. For example, IP6K generated 5-IP7 modulates their target proteins' functions by; i) binding or; ii) pyrophosphorylation [19,20,27]. In addition, inositol pyrophosphates regulate cellular polyphosphate levels [28]. Moreover, IP6Ks regulate certain metabolic and neuronal targets by direct protein–protein interaction, which does not require catalytic activity [29–31].

IP6K1 regulates energy metabolism by modulating diverse pathways, such as, insulin secretion, insulin signaling, glycolysis and energy expenditure (EE) [32–34]. IP6K1 knockout (IP6K1-KO) mice are protected against HFD-induced weight gain, insulin resistance, hyperglycemia, hyperinsulinemia, hyperleptinemia, hypercholesterolemia, and fatty liver [32]. 5-IP7 promotes insulin resistance in DIO mice by inhibiting the insulin sensitizing protein kinase Akt in metabolic tissues [32]. Akt maintains glucose homeostasis via diverse mechanisms [19,35–37]. Therefore, Akt2-KO mice display diabetes like syndrome [38]. Conversely, skeletal muscle-specific overexpression of constitutively active Akt1 protects mice from HFD-induced weight gain [39]. Moreover, Akt mediated M2 macrophage survival increases insulin sensitivity and thermogenesis [40]. Accordingly, Akt activation is impaired in obese/diabetic rodent/human subjects [37,41–44]. 5-IP7 inhibits Akt by diminishing its membrane translocation and stimulatory phosphorylation [32,45–49]. As a result, HFD-fed IP6K1-KO mice display enhanced Akt mediated insulin sensitivity [32]. IP6K1-KO mice are also protected against HFD-induced weight gain due to increased EE, although the cellular mechanism by which IP6K1 regulates EE is not known [32]. Targeting EE is an attractive approach to combat obesity and T2D [10,12,50,51]. Basal metabolism (60–75%), physical activity (10–20%), and diet/cold induced thermogenesis (10–15%) constitute total EE [52]. An enhancement in any of these processes promotes weight loss.

Therefore, it is conceivable that pharmacologic inhibition of IP6K1 enhances insulin sensitivity and EE in DIO mice, although this exciting possibility has not been explored yet. The compound TNP [N2-(m-Trifluorobenzyl), N6-(p-nitrobenzyl)purine] [53] is an IP6K inhibitor [54]. TNP is 70-fold more potent on IP6Ks over its other target IP3-3K [54]. Moreover, TNP does not influence the other IP7 (1-IP7) generating enzyme PP-IP5K [55] or 71 unrelated kinases; thus, it is specific to IP6Ks [54]. Accordingly, TNP reduces 5-IP7 levels in various cells including adipocytes [19,32,45,54,56,57]. Furthermore, 5-IP7 is the precursor of PPIP5K mediated production of the higher inositol pyrophosphate 1,5-IP8 [22,55]. Accordingly, TNP reduces both 5-IP7 and 1,5-IP8 levels in NIH3T3 cells [58]. Depending on cellular energy status, IP6Ks phosphorylate or dephosphorylate IP6 [26]. TNP inhibits IP6K's kinase and phosphatase activities [26,54]. As a result, TNP mediated inhibition of IP6Ks leads to a corresponding increase in the substrate (IP6) level [32,58].

Various reports suggest that TNP mediated IP6K inhibition enhances Akt activity [32,45,56,57]. TNP enhances IGF-1 mediated Akt phosphorylation in the WT mouse embryonic fibroblast cells (MEF) [32]. Conversely, IGF-1 stimulates Akt to a higher extent in IP6K1-KO MEF which is not further augmented by TNP [32]. This observation suggests that TNP inhibits Akt via IP6K1 inhibition [32]. Furthermore, 5-IP7 is elevated in aged mesenchymal stem cells (MSC) [57]. TNP mediated inhibition of 5-IP7 stimulates Akt which diminishes apoptosis in these cells [57]. Finally, a recent study elegantly demonstrates *in vivo* efficacy of TNP in protecting cardiac ischemia reperfusion injury (I/R) in diabetic db/db mice [56]. TNP injection for fourteen days in these mice leads to substantial reduction in 5-IP7 levels in the heart of diabetic db/db mice [56]. Moreover, TNP protects cardiac ischemia in these mice via enhancement of Akt mediated survival and AMPK-PGC1$\alpha$ mediated mitochondrial biogenesis [56]. This information prompted us to perform an in-depth study to monitor TNP's effects on body weight and insulin resistance in DIO mice under various conditions. Our study demonstrates that pharmacologic inhibition of IP6Ks has strong anti-obesity and anti-diabetic properties. We establish, for the first time, that the inositol pyrophosphate biosynthetic pathway has therapeutic significance in obesity and T2D.

## 2. MATERIAL AND METHODS

### 2.1. Materials

High Fat Diet was purchased from Bio-Serv, Flemington, NJ, USA (Cat# S3282, 60% fat calories), kits for measuring insulin and glycerol were from Crystal Chem Inc. Downers Grove, IL, USA (Cat # 90080), and Cayman Chemical Company Ann Arbor, Michigan, USA (Cat # 10010755) respectively. Glucose strips were from Bayer, Pittsburgh, PA, USA. Insulin in the form of Novolin-R was purchased from Novo Nordisk Inc., Plainsboro, NJ, USA. Plasma protein equilibrium dialysis and BCA protein estimation kits were from Pierce/Thermo Fisher Scientific, Waltham, MA USA. Protease-phosphatase inhibitors are from Thermo Fisher Scientific. Antibodies against total AKT was from R&D and $\beta$-actin was from Santa-Cruz Biotechnology. All other antibodies were purchased from Cell Signaling Technology. Q-PCR probes are from Taqman. Unless otherwise stated, all chemicals were purchased from Sigma–Aldrich, St. Louis, MO, USA.

### 2.2. Animals

Wild-type (WT) C57BL6 male mice were used for the study. For IP6K1-KO study, seventh generation, inbred IP6K1-KO mice and their corresponding WT littermates were used [30,59]. Mice were housed under barrier conditions with standard chow diet (CD) (Harlan Laboratories # 2018SX) and water provided *ad libitum* for 2 months. At two months of age, animals were fed a HFD and continued as per the different TNP treatment regimen described in the methods section. Animals were maintained at 12 h light–dark cycle at ambient temperature of 23 °C, unless otherwise indicated. Body weight was monitored every week. All protocols were approved by the Scripps Florida, Institutional Animal Care and Use Committee.

### 2.3. TNP synthesis

#### 2.3.1. 2-chloro-6-methoxy-9H-purine (compound 1)

To a solution of sodium (1.65 g, 72 mmol, 1.36 equiv) in MeOH (100 mL) 2,6-dichloro-9H-purine (10 g, 53 mmol, 1 equiv) was added under argon. The mixture was stirred to reflux for 6 h. The reaction was cooled

 © 2016 The Author(s). Published by Elsevier GmbH. This is an open access article under the CC BY-NC-ND license (http://creativecommons.org/licenses/by-nc-nd/4.0/).

to room temperature and stirred at room temperature overnight. Water (50 mL) was added and the mixture was neutralized with a solution of acetic acid. The precipitate was filtered, washed with water, and dried to afford the 2-chloro-6-methoxy-9H-purine as a white solid. $^{1}$H NMR (DMSO-$d_6$, 400 MHz) $\delta$: 8.43 (s, 1H). $^{13}$C NMR (DMSO-$d_6$, 400 MHz): $\delta$: 171.99, 159.48, 150.97, 143.93, 54.70. **MS**: *m/z* 185 $[M+H]^+$.

#### 2.3.2. 2-(3-(trifluoromethyl)benzyl)amino)-9H-purin-6-ol (compound 2)

To a solution of 2-chloro-6-methoxy-9H-purine **1** (1 g, 5.4 mmol, 1 equiv) in DMAC (20 mL) (3-(trifluoromethyl)phenyl)methanamine (1.5 g, 10.8 mmol, 2 equiv) and triethylamine (2 equiv) were added under argon. The mixture was stirred at 150 °C overnight. The reaction was cooled to room temperature, water was added, and the organic layer was extracted with EtOAc. The combined organic layers were washed with brine and dried over $Na_2SO_4$. The filtrate was evaporated in *vacuo* to obtain the crude, which was purified by flash chromatography (EtOAc/Hex) to provide the title compound **2**. $^{1}$H NMR (DMSO-$d_6$, 400 MHz) $\delta$: 12.46 (s, 1H, NH), 10.68 (s, 1H, OH), 7.68 (s, 1H), 7.57–7.62 (m, 3H), 6.88 (m, 1H), 4.57 (d, $J = 5.9$ Hz, 2H). $^{13}$C NMR (DMSO-$d_6$, 400 MHz): 156.95, 141.05, 131.20, 129.41, 129.20, 128.89, 125.65, 123.60, 123.56, 123.52, 122.94, 43.41. **MS**: *m/z* 310 $[M+H]^+$.

#### 2.3.3. N6-(4-nitrobenzyl)-N2-(3-(trifluoromethyl)benzyl)-9H-purine-2,6-diamine (TNP)

2-((3-(trifluoromethyl) benzyl)amino)-9H-purin-6-ol **2** (500 mg, 1.6 mmol, 1 equiv) was dissolved in phosphoryl chloride (5 mL) and stirred at 100 °C for 1 h. The reaction was cooled to room temperature, and the solution was concentrated *in vacuo* to afford the compound **3** as a light yellow oil, which is directly used in the next step. To a solution of 6-chloro-N-(3-(trifluoromethyl)benzyl)-9H-purin-2-amine **3** (500 mg, 1.5 mmol, 1 equiv) in DMAC (20 mL) was added (4-nitrophenyl)methanamine (302 mg, 1.6 mmol, 1.05 equiv) and triethylamine (2 equiv) under argon. The mixture was stirred at 90 °C overnight. Water was added, and the organic layer was extracted with EtOAc. The combined organic layers were washed with brine and dried over $Na_2SO_4$. The filtrate was evaporated in *vacuo* to obtain the crude, which was purified by flash chromatography (EtOAc/Hex) to provide **TNP** as an orange powder. $^{1}$H NMR (DMSO-$d_6$, 400 MHz) $\delta$: 12.22 (s, 1H, NH), 8.07 (m, 2H), 7.69 (s, 1H), 7.60 (m, 2H), 7.47–7.50 (m, 3H), 6.97 (m, 1H), 4.66 (s, 2H), 4.46 (d, $J = 5.9$ Hz, 4H). $^{13}$C NMR (DMSO-$d_6$, 400 MHz): 170.31, 156.85, 155.16, 155.07, 152.31, 151.16, 149.63, 140.99, 135.44, 135.40, 131.15, 129.40, 128.85, 123.55, 123.51, 122.97, 59.72, 43.38. **MS**: *m/z* 444 $[M+H]^+$.

### 2.4. IP6K1 activity assay *in vitro*

#### 2.4.1. Radiochemical assay

Recombinant human IP6K1 (100 ng) was assayed in a reaction mixture of 20 μl containing 20 mM Tris (pH 7.4), $MgCl_2$ (5 mM), IP6 (2 nmol), [3H]IP6 (130 nCi), ATP (1 mM) and DTT (1 mM) [24,60]. After 1 h, 5-IP7 formed were resolved by HPLC. To monitor TNP's effects, DMSO or TNP (1 μM) was added in the assay. IP6K1 activity in presence of DMSO was considered as 100%.

#### 2.4.2. SDS-PAGE assay

Effect of TNP on recombinant human IP6K1 was also determined by the SDS-PAGE assay, following a standard procedure [61]. Recombinant human IP6K1 (100 ng) was used in a reaction mixture of 20 μl containing 20 mM Tris (pH 7.4), $MgCl_2$ (5 mM), IP6 (5 nmol), ATP (1 mM) and DTT (1 mM). To monitor TNP's effects, DMSO or TNP (1 μM) was added in the assay.

### 2.5. TNP injection in mice

TNP was dissolved in DMSO:Tween 80:water (1:1:8). Although TNP injection in mice is not common, one study successfully injected the compound in mice intraperitoneally [56]. Therefore, dose was selected based on plasma and tissue availability following a single intraperitoneal TNP injection (20 mg/kg BW). Effects of the same dose of TNP on GTT was also tested. Based on this information, the dosing was finalized, and the following studies were designed.

#### 2.5.1. Single dose of TNP (vehicle-n = 4, TNP-n = 4)

A single dose (20 mg/kg; body weight) of TNP was injected in chow(CD)-fed lean and DIO mice. After the treatment, mice were fasted for 5 h, after which GTT was performed. Thereafter, mice were sacrificed for tissue collection.

#### 2.5.2. Short-term (SREV-TNP: vehicle-n = 6, TNP-n = 8)

Mice were fed a HFD for 8-weeks, after which they were treated with TNP (20 mg/kg BW; daily) while HFD was continued. After 7 days of treatment, food intake was measured. GTT and ITT were performed on the 12th and 17th days of injection. QNMR was performed before and after TNP treatment. Mice were sacrificed on day 18, and tissues were collected.

#### 2.5.3. Long-term TNP for protection against DIO (Pro-TNP: vehicle-n = 6, TNP-n = 6)

TNP treatment (10 mg/kg BW; daily) and HFD were started simultaneously and continued for 10 weeks. Body weight was measured weekly. A series of metabolic experiments were done in the following order: EE in the 5th week (when average body weight of vehicle and TNP treated mice were ~30 g and 28 g respectively); food intake on the 7th week; GTT on the 8th week and ITT on the 9th week. A gap of at least one week was maintained between experiments to avoid stress. QNMR was performed before treatment and at the 4th and 10th weeks of treatment. After 10-weeks, TNP treatment was stopped, but HFD was continued for another 8-weeks. GTT was performed 2 and 4-weeks after TNP-withdrawal. No tissue was collected from this experiment.

#### 2.5.4. Long-term TNP for reversal of DIO in WT and IP6K1-KO mice (Rev-TNP: WT-vehicle: n = 4, WT-TNP: n = 4; KO-vehicle: n = 4, KO-TNP: n = 4)

DIO was generated in WT and IP6K1-KO mice by feeding mice a HFD for 8-weeks. After that, TNP was injected (10 mg/kg BW; daily) for 10 weeks along with HFD feeding. GTT was assessed after 5-weeks of TNP treatment. After 10-weeks, NMR was done and mice were sacrificed.

### 2.6. Blood collection and assessment of serum metabolic parameters

For all experiments, animals were sacrificed after 5 h fasting. Blood was collected by cardiac puncture, and serum was prepared following standard procedure. Serum cholesterol, TAG, HDL, LDL, AST, and ALT were measured at the TSRI metabolic core facility. Serum insulin concentration was determined by using an ultra-sensitive mouse ELISA kit.

### 2.7. Body composition analyses by Q-NMR

Fat, lean and fluid masses of DIO mice were measured using the Minispec LF-NMR (Brucker Optics) analyzer as indicated.

 © 2016 The Author(s). Published by Elsevier GmbH. This is an open access article under the CC BY-NC-ND license (http://creativecommons.org/licenses/by-nc-nd/4.0/). 

### 2.8. CLAMS

Mice were placed individually in metabolic cages with a precise thermostatic control in a Comprehensive Laboratory Monitoring System (CLAMS; Columbus Instruments) and were acclimatized for 36 h. Afterwards, $VO_2$, $VCO_2$ and spontaneous locomotor activity were measured for 48 h. Respiratory exchange ratio (RER) and EE were calculated using the following equations: RER $= VCO_2/VO_2$, EE (kcal/h) $= (3.815 + 1.232*RER)*VO_2$. Values were normalized by lean body mass [62].

### 2.9. Glucose and insulin tolerance tests (GTT and ITT)

GTT and ITT were performed in 5 h fasted mice following previously published procedure [32]. For GTT, and ITT, glucose (2 g/kg BW; i.p.) and human recombinant insulin (0.75 U/kg BW; i.p.), respectively, were injected intraperitoneally. After injection, blood was taken by puncturing the tail vein, and glucose levels were measured using a glucometer at indicated time periods. Blood glucose was also measured before the injection (time point 0).

### 2.10. Food intake studies

Food intake was monitored using the BioDAQ instrumentation (Research diet) following the vendor's recommendations. Mice were acclimatized for 2 days. Afterwards, food consumption of each mouse was recorded for 4 consecutive days. Meal is defined as food intake of 0.1 g or more within 900s, which is the gap between feeding bouts. Calorific intake was measured using the calculation: 1 g = 3.1 Kcal.

### 2.11. Thermoneutral studies

For thermoneutral studies, mice were fed a HFD for 6-weeks at 23 °C. Afterwards, they were acclimatized at 30 °C for 2-weeks on HFD. Thereafter, vehicle or TNP was injected for another 8 weeks. Body weight was measured weekly. Insulin sensitivity was measured after 4-weeks of TNP injection. After 8-weeks of injection, mice were-sacrificed to collect tissue samples.

### 2.12. Long-term TNP treatment on fertility of chow-fed male mice

Six-week old chow-fed males were treated with TNP (10 mg/kg BW; daily) for 4 weeks. After that, these mice were used for breeding while TNP injection was continued for additional 11 weeks (total 15 weeks). Each TNP-male participated in 4-rounds of harem breeding, of which the last breeding was after 14-week of treatment.

### 2.13. RNA isolation and real time PCR

RNA isolation was done using the traditional Trizol method. cDNA was synthesized by Qscript (Quanta). Quantitative gene expression was performed using TaqMan primer-probes. mRNA expression was determined using the ΔΔCT method and normalized to the housekeeping gene HPRT.

### 2.14. Histology

Various adipose tissue depots and right lobe of the liver tissue were sent to Scripps Histology core, after appropriate fixation for two days in 10% neutral buffered formalin. Eight micron-sections were prepared and subsequently stained with hematoxylin and eosin (H&E). For UCP1 immunohistochemistry, DAB stain was used. Adipocyte size was quantified using ImageJ software.

### 2.15. Nissl stain

Nissl stain and stereology of brain sections were performed following a standard procedure [63]. Briefly, whole brain was fixed in 10% neutral buffered formalin, and soaked in 30% sucrose. Coronal brain sections (50 μm) were obtained from the whole rostro-caudal extent of the hippocampus, using a sliding microtome. Nissl-staining was performed by submerging mounted sections in cresyl violet for 20 min prior to dehydration. Stereological counts of Nissl-stained cells were performed, using Stereo Investigator software (MicroBrightField Inc, Williston, VT). Measurements were performed on every sixth Nissl-stained coronal sections, extending from the most-rostral to the most-caudal parts of the hippocampus. Both hemispheres of a given brain were analyzed separately. Striatal volume was quantified according to a previously described method [64]. The number of neurons in each CA1 (cornus ammnonis) area was estimated using a fractionator sampling method. For each stereological probe (16–20 probes for each brain), CA1 neurons were counted within a counting frame of 25 × 25 μm (a sampling site), and 10–15 sampling sites were randomly picked by the software within the outlined area. The counts were then extrapolated to estimate the total number of neurons in the CA1 area. For all probes, the coefficient of error (CE Scheaffer) was <1.

### 2.16. Glycerol assay for lipolysis

Mouse serum was used to measure glycerol concentration as per manufacturer's instructions. For cell culture, 3T3-L1 preadipocytes were differentiated for 7 days in a 12-well plate following a standard protocol [32]. Lipolysis was measured following a standard procedure [29]. Briefly, adipocytes were incubated with DMSO or TNP (1 μM) for 4 h in DMEM containing 0.5% BSA (fatty acid free). Afterwards, media was changed, and fresh media was added with or without isoproterenol (IsoP; 10 μM). TNP treatment was continued throughout the assay. Cell culture media was used for glycerol assay using the same kit described above.

### 2.17. Gel Electrophoresis and Immunoblotting

For immunoblotting, protein was isolated by standard protein lysis RIPA buffer, containing the protease-phosphatase inhibitor tablet (Thermo-Scientific), and quantified using a BCA protein assay kit (Pierce). Immunoblotting was done following the standard procedure [32]. To detect Akt phosphorylation, both T308 and S473 antibodies were used in single-dose TNP treated IWAT samples. For other samples/tissues, only Akt-S473 were detected. Densitometric analyses of protein bands were performed by quantifying them (n = 3), using the ImageJ software.

### 2.18. TNP DMPK

Following DMPK properties of TNP were analyzed.

#### 2.18.1. Plasma protein binding (PPB)

Plasma binding. Plasma protein binding was determined using equilibrium dialysis. All samples were tested in triplicate, using the RED Rapid Equilibrium Dialysis Device (Thermo Scientific). The initial drug concentration in the plasma chamber was 1 μM and phosphate buffered saline was added to the receiver chamber. The plate was covered and allowed to shake in a 37 °C incubator for 6 h 25 μl was sampled from the plasma and PBS chambers, which were then diluted with either blank PBS or plasma to achieve a 1:1 ratio or plasma:PBS for all samples. The concentration of drug in the plasma and PBS chambers was determined by LC-MS/MS. The fraction bound was calculated as ([plasma] − [PBS])/[plasma].

#### 2.18.2. CYP450 inhibition

To understand the potential for common drug–drug interactions, P450 inhibition for four major human isoforms were evaluated in human

 © 2016 The Author(s). Published by Elsevier GmbH. This is an open access article under the CC BY-NC-ND license (http://creativecommons.org/licenses/by-nc-nd/4.0/).

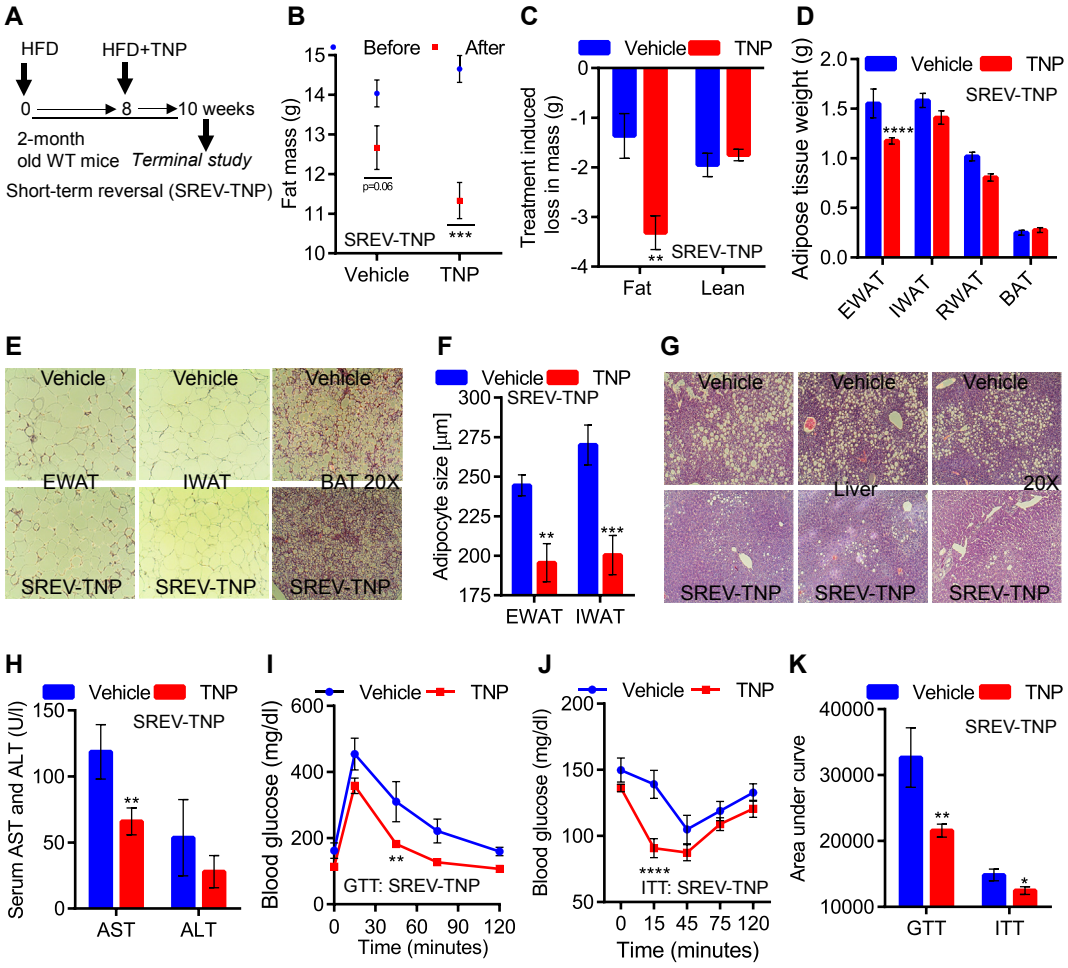


**Figure 1: Short-term IP6K inhibition restores insulin sensitivity and reduces fat accumulation in DIO mice**. A. Study design: Short-term treatment of DIO mice with TNP to monitor reversal of obesity and insulin resistance (SREV-TNP; vehicle: n = 6; TNP: n = 8). B. TNP-mice display a substantial reduction in fat mass compared to vehicle-group (*t-test*). C. Treatment induced reduction in fat mass is higher in TNP-mice whereas lean mass is reduced to a similar extent in both vehicle- and TNP-mice (*t-test*). D. Weight of the EWAT depot of SREV-TNP mice is significantly less whereas IWAT and RWAT are marginally reduced (*t-test*). E. Adipocyte size is smaller in SREV-TNP EWAT and IWAT. SREV-TNP treated BAT accumulates less fat. F. Quantification of adipocyte size in vehicle and SREV-TNP EWAT and IWAT (*t-test*). G. SREV-TNP treatment ameliorates fatty liver in DIO mice. Numerous white vacuoles (which represent fat droplets) are visible in DIO vehicle treated mice whereas SREV-TNP mice display substantially less number of droplets. H. Serum levels of hepatotoxic enzymes aspartate transaminase (AST) and alanine aminotransferase (ALT) are less in SREV-TNP mice (*t-test*). I. Efficient glucose disposal following glucose (GTT) injection in SREV-TNP-mice (*Two way Anova*). J. SREV-TNP mice also display enhanced glucose disposal following insulin injection (ITT) (*Two way Anova*). K. AUC values confirm improved glucose disposal in SREV-TNP mice in GTT and ITT tests (*t-test*).

hepatic microsomes, by following the metabolism of specific marker substrates (CYP1A2 phenaceten demethylation to acetaminophen; CYP2C9, tolbutamide hydroxylation to hydroxytolbutamide; CYP2D6, bufuralol hydroxylation to 4′-hydroxybufuralol; and CYP3A4, midazolam hydroxylation to 1′-hydroxymidazolam) in the presence or absence of 10 µM probe compound. The concentration of each marker substrate is approximately its Km. Specific inhibitors for each isoform were included in each run to validate the system.

### 2.18.3. Hepatic microsomal stability

Evaluated by incubating TNP (1 µM) with hepatic microsomes (1 mg/ml) and 1 mM NADPH in potassium phosphate (100 mM, pH 7.4); aliquots were removed at 0, 5, 10, 20, 40, and 60 min and analyzed by LC-MS/MS, represented as half-life.

### 2.19. Statistics

Trial/prior experiments were used to determine sample size with ample statistical power. To obtain statistically significant data, n = 6–8 animals/group were used for phenotypic characterization. For mechanistic experiments such as WT, IP6K1-KO comparison, and single-dose TNP, n = 3–4 animals/group were used. Animals were excluded from experiments if they showed any sign of sickness. Number of mice (n) used in experiments is indicated in the legend. Immunoblots were quantified using 'ImageJ' software. For multiple comparisons, one/two-way Anova was used. For two independent data sets, two-tailed Student's *t-test* was used. Data are presented as mean ± SEM (****P ≤ 0.0001, ***P ≤ 0.001, **P ≤ 0.01 and *P ≤ 0.05). Statistical significance was calculated in GraphPad Prism, version 6.

## 3. RESULTS

### 3.1. Short-term IP6K inhibition restores insulin sensitivity and reduces fat accumulation in DIO mice

TNP was synthesized in the laboratory (Supplemental Figure 1A–M). To test TNP's effects on IP6K1, recombinant human IP6K1 was purified

 © 2016 The Author(s). Published by Elsevier GmbH. This is an open access article under the CC BY-NC-ND license (http://creativecommons.org/licenses/by-nc-nd/4.0/). 

[30] (Supplemental Figure 1N) and its catalytic activity was confirmed (Supplemental Figure 1O). The compound, at 1 μM, blocks the catalytic activity of IP6K1 *in vitro* (Supplemental Figure 1P and Q). Next, we monitored TNP's plasma and tissue availability. Following a single injection (20 mg/kg BW) in chow-fed (CD) mice, we detected 5 μM of TNP in plasma, 6 h post-administration (Supplemental Figure 1R). TNP is accumulated at ~10–25 μM in liver, skeletal muscle, and adipose tissue depots, although its accumulation in the brain is considerably less (0.63 μM; Supplemental Figure 1S).

Thereafter, we determined effects of short-term TNP (20 mg/kg BW; daily for 18 days) treatment on DIO mice (short-term reversal; SREV-TNP; Figure 1A). Comparison of body weight before and after injection, reveals that TNP-mice display a marginally higher reduction in body weight than the vehicle-group (Supplemental Figure 2A). The slight reduction in body weight is due to a decrease in fat mass of TNP-mice (Figure 1B). TNP reduces ~3 g whereas vehicle decreases ~1 g of fat (Figure 1C; fat). Lean mass is reduced to a similar extent in both groups (Figure 1C; lean). Accordingly, weight of the epididymal white adipose tissue depot (EWAT) is less in SREV-TNP mice (Figure 1D). Other depots, such as inguinal and retroperitoneal adipose tissue (IWAT and RWAT) but not BAT, display marginal reduction (Figure 1D). Adipocyte size in the EWAT and IWAT of SREV-TNP mice is also reduced (Figure 1E,F). Vehicle-BAT accumulates substantial amount of fat, which is evidenced by presence of numerous vacuoles in the histological preparation (Figure 1E; BAT-vehicle). However, SREV-TNP treated mice accumulate much less fat in the BAT (Figure 1E; BAT-

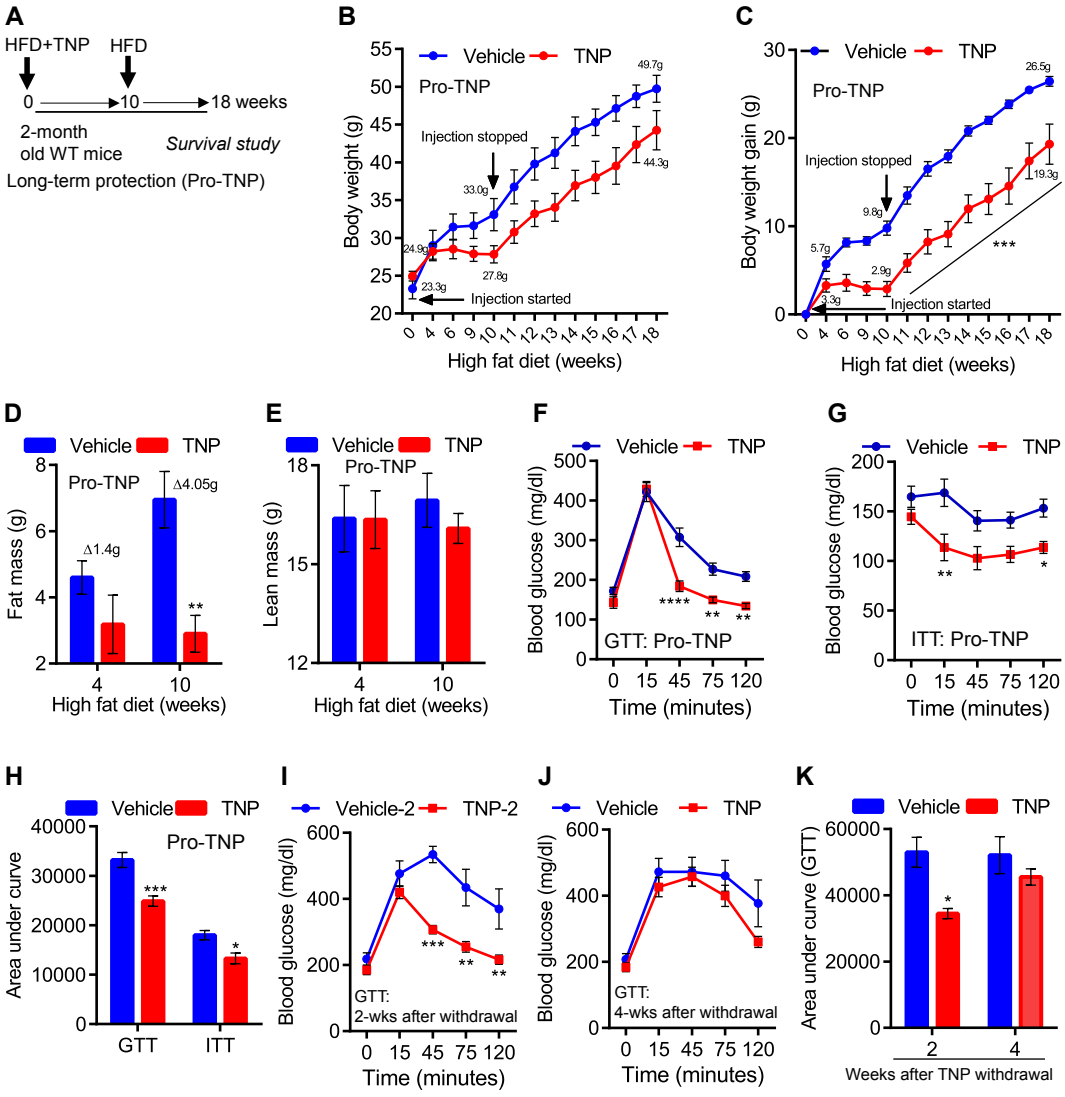


**Figure 2: IP6K, when inhibited at the onset of HFD feeding, protects mice from DIO and insulin resistance**. A. Study design: protection from DIO by long-term TNP treatment (Pro-TNP) (n = 6/group; total two groups). B. At the onset of the experiment, body weight of vehicle- and TNP-group was 23.3 g and 24.9 g, respectively. After 10-weeks of HFD, vehicle-group has an average body weight of 33.0 g whereas the TNP-group has an average body weight of 27.8 g. At this point, injection was stopped. Eight-weeks after withdrawal, body weight of vehicle-mice was 49.7 g compared to 44.3 g in TNP-mice (*Two way Anova*). C. Pro-TNP-mice gain body weight at a substantially lower rate during 10-weeks of injection period. After TNP is withdrawn, both vehicle and Pro-TNP group gained body weight at a similar rate (*Two way Anova*). D. Fat mass is less in Pro-TNP-mice after 4- and 10-week of treatment (*t-test*). E. Lean mass is unaltered in Pro-TNP mice (*t-test*). F and G. Pro-TNP-mice display efficient glucose disposals following glucose (GTT) and insulin injections (ITT) (*Two way Anova*). H. AUC analyses of Figure 2F,G (*t-test*). I. TNP-withdrawn mice exhibit efficient glucose disposal following glucose injection (GTT), 2 weeks after withdrawal (TNP-2). Vehicle-withdrawn (vehicle-2) mice are glucose intolerant (*Two way Anova*). J. Four-weeks post-withdrawal, Pro-TNP group become glucose intolerant (TNP-4) similar to vehicle-mice (vehicle-4) (*Two way Anova*). K. Area under curve analyses for Figure 3H,I (*t-test*).

 © 2016 The Author(s). Published by Elsevier GmbH. This is an open access article under the CC BY-NC-ND license (http://creativecommons.org/licenses/by-nc-nd/4.0/).

SREV-TNP). IP6K1 regulates lipolysis by directly interacting with the lipolytic regulator protein perilipin1 which does not require its enzyme activity [29]. Accordingly, TNP does not alter glycerol release in mice or in 3T3L1 adipocytes (Supplemental Figure 2B and C). Fat accumulation is also less in SREV-TNP liver (Figure 1G) which protects mice from HFD-induced hepatotoxicity (Figure 1H). Serum levels of cholesterol or triglycerides are not altered in this condition (Supplemental Figure 2D and E).

IP6K1 promotes whereas TNP inhibits insulin secretion [33,54]. Conversely, IP6K1 inhibits while TNP stimulates the insulin effector protein kinase Akt [32,57]. As a result, IP6K1-KO mice are insulin hypersensitive despite having less insulin in the serum [32,59]. Therefore, we presume that TNP improves glucose/insulin homeostasis in DIO mice. Indeed, short-term TNP-mice display efficient glucose disposal following exogenous glucose injection (Figure 1I,K; GTT). Improved GTT in TNP-mice is presumably due to i) increased glucose induced insulin secretion or ii) enhanced insulin sensitivity in metabolic tissues. However, serum insulin level is largely similar in vehicle and TNP-mice under this condition (Supplemental Figure 2F). Moreover, exogenous insulin treatment disposes glucose more efficiently in TNP-mice (Figure 1J,K; ITT), which indicates that insulin sensitivity is enhanced by TNP treatment, which is further evidenced in the following sections.

### 3.2. IP6K, when inhibited at the onset of HFD feeding, protects mice from DIO and insulin resistance

Although the above results are encouraging, they do not answer whether TNP treatment is efficient to decelerate initiation of DIO and insulin resistance over a prolonged period of time. To test this, TNP treatment (10 mg/kg BW; daily) was started at the onset of HFD feeding and continued for 10 weeks. Furthermore, to monitor whether TNP mediated changes are reversible, the treatment was stopped after 10 weeks, but HFD was continued for another 8-week (Figure 2A; Protection Long-term; Pro-TNP). At the onset of the experiment, body weight of vehicle-treated and TNP-treated animals was 23.3 g and 24.9 g, respectively (Figure 2B). After 10-week of HFD, the vehicle group displayed an average body weight of 33.0 g whereas the TNP group exhibited 27.8 g (Figure 2B; 10-week). At this point, injection was stopped, but HFD was continued. Eight-weeks after drug withdrawal, body weight of vehicle-mice was 49.7 g compared to 44.3 g in TNP-mice (Figure 3B; 18-week). Thus, after 10 weeks, TNP-mice gained ~one-third of their body weight compared to vehicle-mice (2.9 g in TNP vs 9.8 g in vehicle) (Figure 2C; injection stopped). TNP mediated reduction is reversible as the TNP-group started gaining weight at a rate comparable to vehicle-mice when the treatment was stopped after 10 weeks. After TNP-withdrawal, the vehicle-group gained 26.5 g (from 9.8 g) whereas the Pro-TNP mice gained 19.3 g (from 2.9 g) (Figure 2C; 18-week). Therefore, weight—gain in vehicle and (16.7 g) TNP-withdrawn mice (16.4 g) is comparable during the withdrawal period.

Pro-TNP treatment reduces body weight by diminishing fat accumulation without altering lean mass (Figure 2D,E). Moreover, TNP treatment delays the onset of insulin resistance and hyperglycemia. Thus, both glucose and insulin induced glucose disposals are improved in Pro-TNP mice (Figure 2F—H). Conversely, TNP-removal gradually leads to insulin resistance. After 2-week of removal, Pro-TNP mice still display improved glucose disposal (Figure 2I,K; GTT-2 weeks after withdrawal) whereas after 4-week, they become insulin resistant similar to vehicle-TNP mice (Figure 2J,K; GTT-4 weeks after withdrawal). Thus, long-term TNP treatment decelerates initiation of DIO and insulin resistance in a reversible manner.

### 3.3. TNP promotes weight loss and restores metabolic homeostasis in DIO mice *via* specific inhibition of IP6K1

From the above experiment, it is clear that TNP reduces initiation of DIO. Next, we asked, i) does long-term TNP reverse the symptoms of DIO and insulin resistance, and ii) does the compound exert its effects, at least in part, via regulation of the IP6K1 pathway? To test this, DIO was generated by feeding IP6K1-KO mice and their WT littermates a HFD for 8-weeks (Figure 3A). After 8-weeks of HFD-feeding, WT mice gained ~16.2 g (42.4 g from 26.2 g; Figure 3B). IP6K1-KO mice are partly protected against DIO [32]. Therefore, the knockouts gained ~8.8 g (31.8 g from 23 g; Figure 3C). Thereafter, mice were treated with TNP (10 mg/kg BW; daily) for 10-week (Figure 3A; Rev-TNP). After 10-week of treatment (total 18 weeks), TNP-WT mice display a reduction of ~10 g in body weight (46.5 g vehicle vs 36.9 g TNP; Figure 3B). Conversely, body weight of vehicle and TNP treated IP6K1-KO mice are same after 10-week of treatment (~33 g; Figure 3C). Thus, IP6K1-KO mice are resistant to TNP mediated weight loss (Figure 3C). After 18-week of HFD, IP6K1-KO mice gain 10 g body weight (33—23 = 10 g) compared to 20 g in WT (46.5—26.2 = 20.3 g) (Figure 3B,C). Clearly, the 10 g weight gain in IP6K1-KOs is IP6K1 independent, which is not reduced by TNP treatment. Accordingly, vehicle and TNP treated IP6K1-KO mice look similar whereas TNP treated WT mice appear substantially leaner than their vehicle controls (Figure 3D). Total fat mass is significantly reduced in TNP treated WT compared to vehicle treated mice (Figure 3E). Although IP6K1-KO mice accumulate ~5—6 g of fat, it is not reduced by TNP (Figure 3F). Weight of various adipose tissue depots in WT is also reduced by TNP treatment (Figure 3G). HFD-fed KOs accumulate less fat in various adipose tissue depots than WT [32] (Figure 3G,H). Yet, the KOs accumulate a fair amount, which is not further reduced by TNP (Figure 3H).

Moreover, TNP enhances glucose disposal in WT (Figure 3I,J) but not in IP6K1-KO mice (Figure 3K,L) (GTT; measured after 5 weeks of TNP treatment). TNP also reduces fasting blood glucose (derived from the '0' time point of GTT) in WT mice to the IP6K1-KO level whereas the knockouts are unaffected (Figure 3M). Serum insulin level in WT mice is significantly reduced by TNP, which resembles IP6K1-KOs (Figure 3N; WT). As reported previously [32], IP6K1-KO mice are protected from HFD-induced hyperinsulinemia (Figure 3N; WT vs KO; vehicle). TNP does not further reduce insulin level in IP6K1-KO mice (Figure 3N; KO). These results further indicate that TNP reduces insulin secretion whereas enhances insulin sensitivity. Furthermore, TNP reduces serum cholesterol level in WT mice (Figure 3O; WT). HFD-fed IP6K1-KO mice exhibit less serum cholesterol, although it is higher than normal (80—100 mg/dl) [65] level. TNP does not reduce cholesterol level in IP6K1-KO mice to normal level (Figure 3O; KO). These experiments strongly suggest that TNP promotes weight loss and restores glucose homeostasis specifically by reversing IP6K1's effects on metabolism.

### 3.4. IP6K inhibition enhances insulin sensitivity in DIO mice *via* Akt activation

We presume that TNP enhances insulin sensitivity via Akt activation similar to what is observed in IP6K1-KO mice. Akt activity is stimulated by mTORC2 and PDK1 mediated phosphorylation at serine 473 (S473) and threonine 308 (T308), respectively [66,67]. Indeed, S473 phosphorylation of Akt is 4-fold higher in SREV-TNP (short-term TNP, described in Figure 1) mice (Figure 4A,B). Short-term TNP treatment enhances insulin sensitivity (Figure 1); thus, enhanced Akt activity may also be an effect of the phenotype. Therefore, we tested whether TNP acutely activates Akt. For this, we assessed Akt activity in DIO mice

 © 2016 The Author(s). Published by Elsevier GmbH. This is an open access article under the CC BY-NC-ND license (http://creativecommons.org/licenses/by-nc-nd/4.0/). 

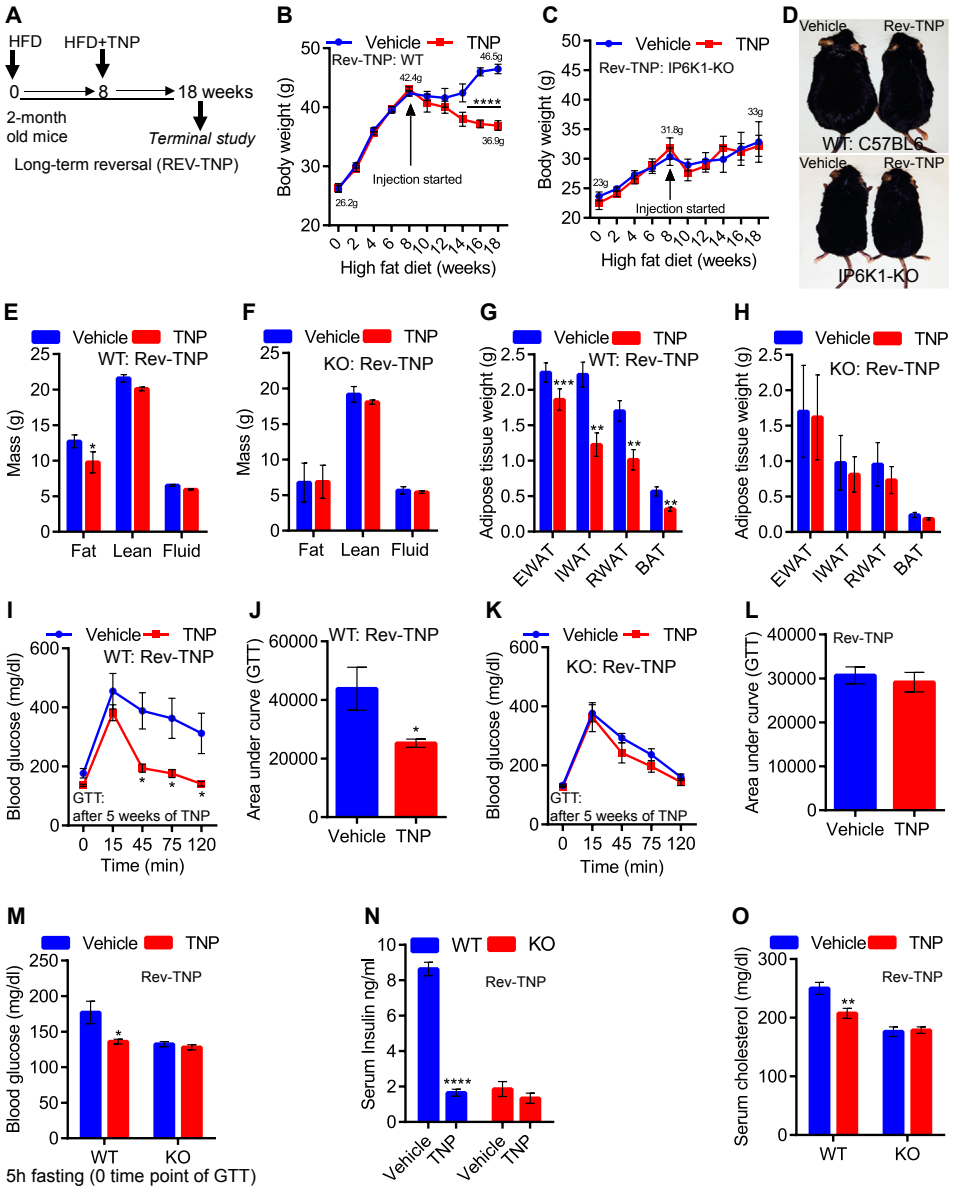


**Figure 3: TNP promotes weight loss and restores metabolic homeostasis in DIO mice *via* specific inhibition of IP6K1**. A. Study design: reversal of DIO by long-term TNP in WT and IP6K1-KO mice (Rev-TNP; n = 4/group; total 4 groups). B. Rev-TNP promotes weight loss in DIO WT mice. After 10-weeks of injection, body weight is 46.5 g in vehicle mice whereas it is 36.9 g in Rev-TNP mice. The average body weight in both groups was ~42.4 g when the injection was started (*Two way Anova*). C. IP6K1-KO mice are resistant to Rev-TNP mediated weight loss (*Two way Anova*). D. Rev-TNP treated WT mice appear smaller in size compared to vehicle-mice. In contrast, both vehicle and Rev-TNP treated IP6K1-KO mice appear similar in size. E. QNMR analysis reveal that total fat mass is significantly less in Rev-TNP WT mice whereas lean and fluid masses are marginally altered (*t-test*). F. Total fat, lean, and fluid masses are unaltered in IP6K1-KO mice following Rev-TNP treatment (*t-test*). G. Rev-TNP treated EWAT, IWAT, RWAT, and BAT exhibit reduced weight in WT mice (*t-test*). H. Rev-TNP does not alter weight of EWAT, IWAT, RWAT, and BAT in IP6K1-KO mice (*t-test*). I and J. TNP enhances glucose disposal in DIO WT mice (GTT) (*Two way Anova* and *t-test*). K and L. Glucose disposal in IP6K1-KO mice is not altered by Rev-TNP treatment (*Two way Anova and t-test*). M. Rev-TNP reduces fasting blood glucose of WT to the level similar to IP6K1-KO mice. IP6K1-KO mice are resistant to TNP induced reduction in blood glucose level (*Two way Anova*). N. Chronic TNP treatment reduces serum insulin level in HFD-fed WT to IP6K1-KO level. IP6K1-KO mice are protected against HFD-induced hyperinsulinemia. TNP does not further reduce serum insulin level in the knockouts (*t-test*). O. TNP reduces serum cholesterol level in WT mice. Although cholesterol levels in IP6K1-KO mice are less than WT, they are higher than the normal range (80–100 mg/dl). However, TNP does not reduce its level to normal in the knockouts (*t-test*).

following a single injection of TNP (20 mg/kg BW). Acute TNP treatment substantially increases stimulatory phosphorylation levels of Akt (T308 and S473) in the IWAT (Figure 4C). We obtained similar results in soleus muscle and liver (Figure 4D,E). Quantification reveals that TNP causes 2–3 fold increase in Akt 473 phosphorylation in these tissues (Figure 4F). Enhanced Akt activity is further evidenced by increased phosphorylation levels of the Akt target GSK3α/β (serine 21/serine 9) in IWAT and muscle (Figure 4G). The same TNP-dose significantly reduces blood glucose level and improves glucose tolerance in DIO mice (Figure 4H,I and 4J). Conversely, a similar dose of TNP does not influence Akt phosphorylation or glucose disposal in CD-fed mice (Supplemental Figure 3A and B). Blood cholesterol, HDL and LDL levels are also lower whereas TAG is not altered by a single TNP dose in DIO mice (Figure 4K). Serum insulin level is enhanced by HFD (Figure 4L;

 © 2016 The Author(s). Published by Elsevier GmbH. This is an open access article under the CC BY-NC-ND license (http://creativecommons.org/licenses/by-nc-nd/4.0/).

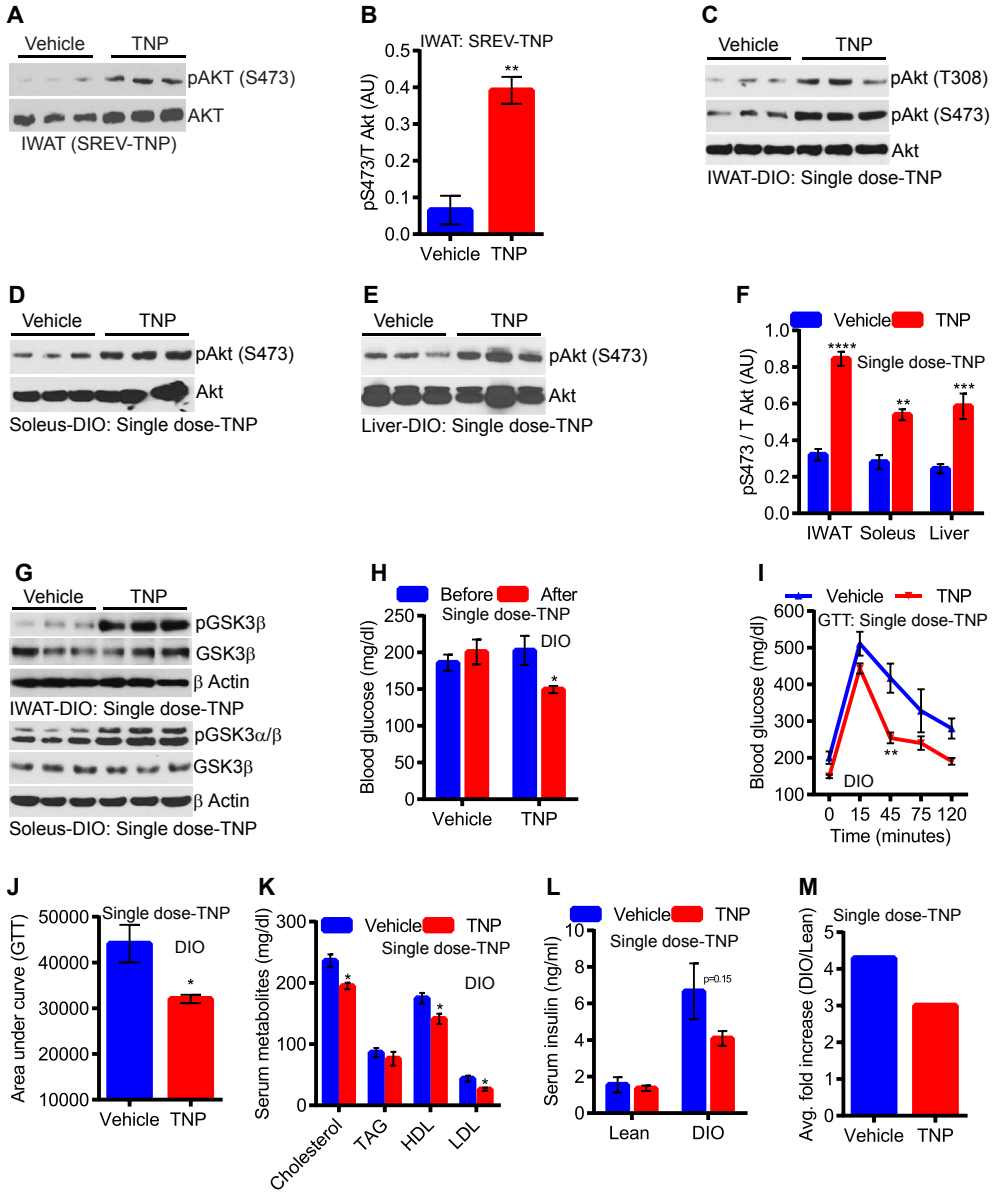


**Figure 4: IP6K inhibition enhances insulin sensitivity in DIO mice *via* Akt activation.** A. SREV-TNP enhances Akt stimulatory (S473) phosphorylation in the IWAT depot. B. Densitometry of Figure 4A reveals that SREV-TNP treatment causes ~4-fold enhancement in the S473 Akt phosphorylation level in the IWAT depot (*t-test*). C. A Single-dose of TNP enhances Akt stimulatory phosphorylation (both T308 and S473) in the IWAT. D and E. TNP enhances Akt phosphorylation (S473) in the soleus muscle and liver. F. ImageJ analyses of phospho S473/total Akt Figure 4C–E reveal that TNP enhances 2–3 fold increase in Akt S473 phosphorylation in the metabolic tissues *(t-test)*. G. A single-dose of TNP also enhances Akt activity on its target GSK3α/β in the IWAT and soleus muscle. H. A single dose of TNP significantly reduces blood glucose level in DIO mice (*t-test*). I. A single dose of TNP significantly improves glucose tolerance in DIO mice (*Two way Anova*). J. AUC analysis of Figure 4I confirms that a single-dose of TNP improved GTT in DIO mice (*t-test*). K. A single dose of TNP slightly reduces serum cholesterol, HDL, and LDL levels whereas it does not influence TAG level (*t-test*). L. HFD enhances serum insulin level. A single dose of TNP slightly reduces HFD induced increase in serum insulin (*t-test*). M. TNP slightly reduces the average fold increase in HFD induced hyperinsulinemia.

blue bars). TNP does not influence insulin level in CD-fed lean mice whereas it slightly reduces HFD induced increase in serum insulin (Figure 4L; red bars; Figure 4M). These results strongly suggest that even a single dose of TNP enhances Akt activity and insulin sensitivity in DIO mice.

### 3.5. TNP treatment promotes weight loss by enhancing the energy expenditure pathways in the adipose tissue

Next, we determined the mechanism by which TNP reduces weight gain. Both long-term (Pro-TNP) and short-term (SREV-TNP) treatments do not influence energy intake in DIO mice (Figure 5A and Supplemental Figure 4A and B). Conversely, Pro-TNP mice display higher $VO_2$ consumption and EE especially during nighttime (Figure 5B–D). Respiratory exchange ratio (RER) and total activity are unaltered (Figure 5E,F).

Brown adipose tissue (BAT) is the primary site for uncoupled respiration mediated thermogenesis [12]. In addition, brown like 'beige' cells in certain WAT depots also display thermogenic properties [50,51]. β3-adrenergic receptor (β3-AR)/PKA signaling pathway stimulates the uncoupling protein 1 (UCP1) which enhances diet/cold

 © 2016 The Author(s). Published by Elsevier GmbH. This is an open access article under the CC BY-NC-ND license (http://creativecommons.org/licenses/by-nc-nd/4.0/). 

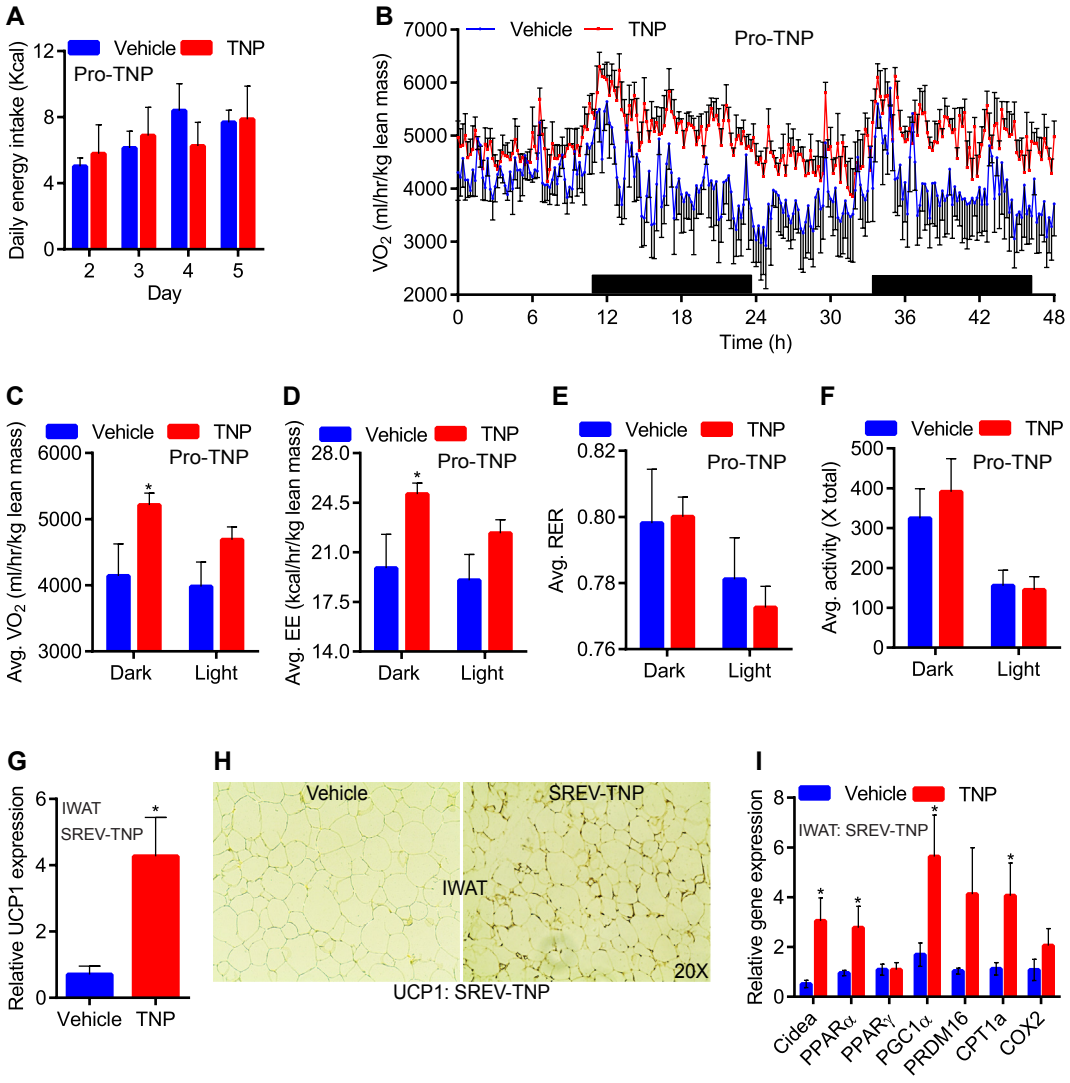


**Figure 5: TNP treatment promotes weight loss by enhancing the energy expenditure pathways in the adipose tissue.** A. Daily energy intake is similar in HFD-fed mice after vehicle or Pro-TNP treatment (*t-test*). B. Pro-TNP mice exhibit higher $VO_2$ consumption. C. Pro-TNP treatment enhances average $VO_2$ consumption especially at night (*t-test*). D. Pro-TNP-mice exhibit higher EE especially during nighttime (*t-test*). E. Average RER is unaltered in Pro-TNP treated mice (*t-test*). F. Average activity is unaltered in Pro-TNP treated mice (*t-test*). G. UCP1 mRNA expression is higher in the IWAT of SREV-TNP mice (*t-test*). H. Immunohistochemistry indicates that UCP1 protein level is higher in SREV-TNP treated IWAT. I. Thermogenic and mitochondrial activity markers such as Cidea, PPARα, PGC1α, PRDM16 and CPT1a are upregulated in SREV-TNP IWAT (*t-test*).

induced thermogenesis in rodents and adult humans [52,68—71]. Accordingly, UCP1 stimulation causes thermogenesis and insulin sensitivity in primates and humans [10,72,73]. UCP1 mRNA and protein levels are substantially higher in SREV-TNP IWAT depot, which indicates that TNP promotes EE at least in part via increasing UCP1 mediated thermogenesis (Figure 5G,H). Expression levels of the other browning marker Cidea is also higher in SREV-TNP IWAT (Figure 5I). Various transcription factors like PPARs and co-activators PRDM16 and PGC1α enhance UCP1 expression [10,51,74]. Accordingly, mRNA levels of these proteins are enhanced in SREV-TNP IWAT (Figure 5I). Mitochondrial fatty acid transporter CPT1a is also higher whereas the cytochrome c oxidase 2 level is marginally increased in SREV-TNP IWAT (Figure 5I). TNP mediated increase in the EE machinery is adipose tissue specific as UCP3 and other markers are largely unaltered in SREV-TNP treated muscle tissue (Supplemental Figure 4C). Furthermore, in long-term TNP-treated WT mice (described in Figure 3) UCP1 expression is increased following TNP treatment (Supplemental Figure 4D; WT). Conversely, UCP1 expression in IP6K1-KO mice is comparable to WT-TNP mice, which is not significantly altered by TNP treatment (Supplemental Figure 4D; KO). Thus, TNP reduces fat accumulation by increasing thermogenic EE. Moreover, TNP enhances UCP1 expression via inhibition of the IP6K1 pathway.

### 3.6. Thermoneutrality partly impacts TNP mediated weight loss without altering its anti-diabetic actions

If thermogenesis is the major, or at least one of the mechanisms, by which IP6K1 regulates EE, it is conceivable that thermoneutrality abolishes TNP mediated weight loss. Therefore, we monitored effects of TNP on body weight and metabolic parameters of DIO mice at thermoneutrality (Figure 6A; reversal of DIO by TNP at thermoneutral temperature; RevT-TNP). At thermoneutrality, TNP blocks weight gain (Figure 6B). Yet, in contrast to ambient (23 °C) temperature (Figure 3B), the compound fails to promote weight loss in DIO mice at thermoneutral temperature (30 °C). Thus, thermoneutrality

 © 2016 The Author(s). Published by Elsevier GmbH. This is an open access article under the CC BY-NC-ND license (http://creativecommons.org/licenses/by-nc-nd/4.0/).

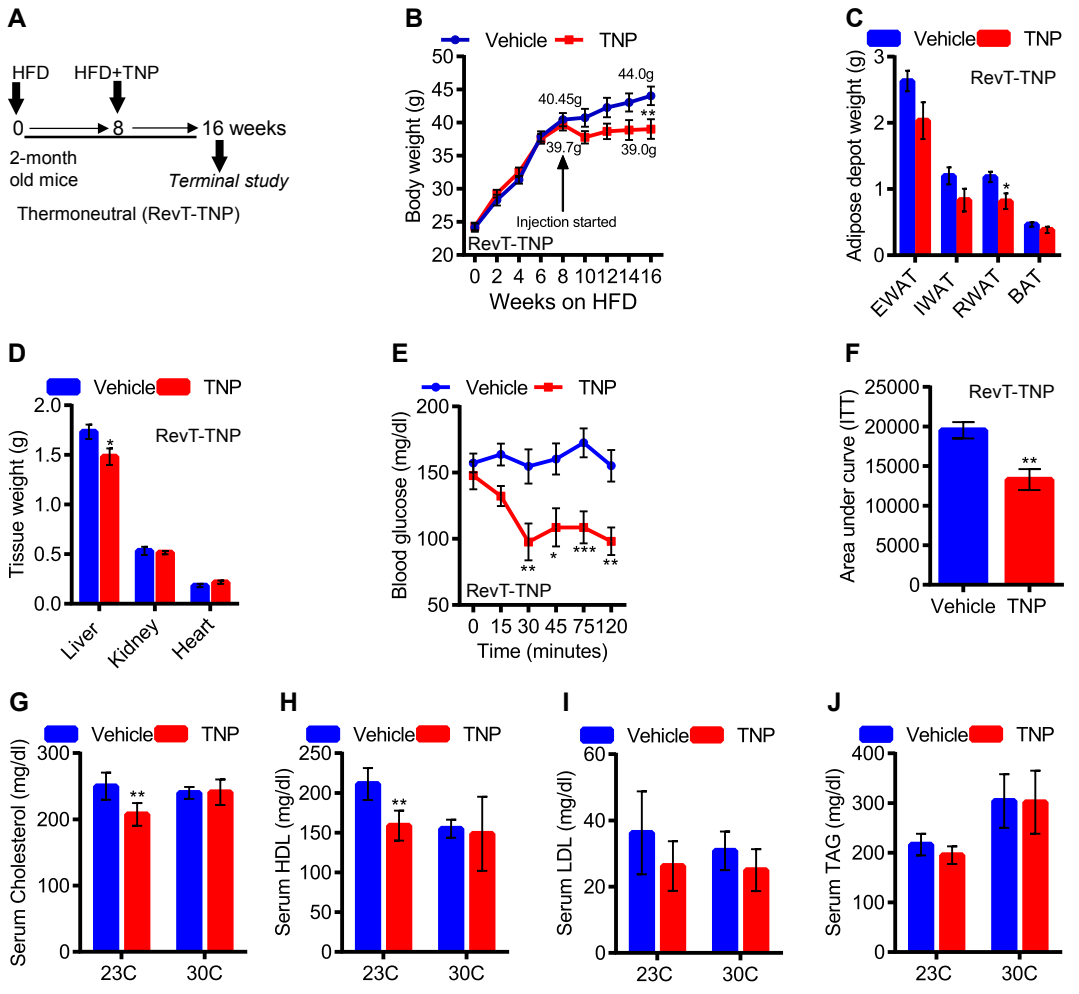


**Figure 6: Thermoneutrality impacts TNP mediated weight loss without altering its anti-diabetic actions.** A. Study design: Effects of long-term TNP treatment on DIO at thermoneutral temperature (RevT-TNP; n = 6/group). B. After 8-weeks of injection, vehicle mice display an average increase of 3.55 g in body weight (44 g from 40.45 g) whereas RevT-TNP mice exhibit an average decrease of ~0.7 g (39 g from 39.7 g) (*Two way Anova*). C. RevT-TNP treated EWAT, IWAT, RWAT, and BAT exhibit slightly reduced weight in DIO mice (*t-test*). D. TNP treatment, at thermoneutral temperature, causes a significant decrease in liver weight. Other organs are not altered (*t-test*). E and F. Thermoneutral-TNP significantly enhances glucose disposal following exogenous insulin treatment (GTT) (*Two way Anova and t-test*). G and H. Serum levels of total cholesterol and HDL are less in TNP-treated mice at ambient temperature whereas they are unaltered at thermoneutral temperature (*t-test*). I and J. Serum levels of LDL and triglycerides are unaltered in TNP-treated mice at both ambient and thermoneutral temperatures (*t-test*).

significantly impacts, although does not completely abolish TNP's effects on body weight. Accordingly, weight of diverse adipose tissue depots are marginally less (Figure 6C) compared to ambient temperature in which TNP substantially reduces adipose tissue weight (Figure 3G). Weight of other tissues such as liver is marginally less whereas kidney and heart do not exhibit any difference (Figure 6D). At this condition, we do not observe any noticeable difference in EE, total activity, and food intake in vehicle and TNP-treated mice (data not shown). Yet, glucose disposal following exogenous insulin treatment (ITT) is significantly improved in RevT-TNP mice (Figure 6E,F). Comparison of other serum metabolic parameters reveals that total cholesterol and HDL is reduced by TNP at ambient but not at thermoneutral temperatures (Figure 6G,H) whereas LDL and TAG levels are unaltered by the compound under both the conditions (Figure 6I,J). Thus, thermoneutrality significantly impacts TNP mediated weight loss. Although TNP does not promote weight loss at thermoneutral conditions, it still protects DIO mice from further weight gain. Moreover, anti-diabetic actions of TNP are not dependent on environmental temperature.

### 3.7. TNP is an encouraging IP6K inhibitor compound, which requires further improvement

Finally, we monitored effects of TNP treatment on other tissues and its drug metabolism and pharmacokinetic (DMPK) properties. Although a detailed analysis of every tissue is beyond the scope of the study, we monitored long-term (Rev-TNP) TNP's impacts on relevant peripheral tissues. Similar to short-term treatment (Figure 1G), long-term TNP-treated mice also display reductions in liver weight and fat accumulation (Supplemental Figure 5A and B). These mice exhibit normal heart and kidney phenotype and weight (Supplemental Figure 5C–E). Testis also appears normal (Supplemental Figure 5F). Male IP6K1-KOs are sterile and display abnormal testis morphology [59]. Therefore, to determine whether long-term TNP affects fertility, we treated chow-fed male WT mice with TNP (10 mg/kg BW; daily) for 15-week. During this time period, TNP-treated males impregnate females (details in the methods section). Testes of these males look normal and healthy (Supplemental Figure 5G). Although TNP does not efficiently cross the BBB, we examined whether its long-term treatment causes neuronal loss in the brain. We focused on neurons in the hippocampal CA1 area,

 © 2016 The Author(s). Published by Elsevier GmbH. This is an open access article under the CC BY-NC-ND license (http://creativecommons.org/licenses/by-nc-nd/4.0/). 

**Table 1** — TNP's stability ($t_{1/2}$) is higher in human microsomes compared to rodents. Plasma protein binding (PPB), PPB is in an acceptable range indicating sufficient free drug fraction for enzyme interaction *in vivo*. Potent human CYP450 inhibition is observed for TNP.

| $cm_pd$ | Microsome stability ($t_{1/2}$ min) | | | % Plasma protein binding | | | CYP450% Inhibition at 10 μM | | | |
|---|---|---|---|---|---|---|---|---|---|---|
| | Human | Mouse | Rat | Human | Mouse | Rat | 1A2 | 2C9 | 2D6 | 3A4 |
| TNP | 32 | 9 | 17 | 91.7 | 90.0 | 93.0 | 86 | 92 | 76 | 98 |

which are very sensitive to insults. Stereological analysis showed no significant difference in neuronal density in the CA1 between WT and IP6K1-KO mice (Supplemental Figure 5H). Furthermore, long-term TNP treatment did not significantly alter CA1 neuronal density in either genotype of mice (Supplemental Figure 5H). These results suggest that long-term TNP treatment does not lead to significant injury to the brain. DMPK studies exhibit that TNP has a half-life ($T_{1/2}$) of 32 min in the human hepatic microsomal stability assay, which suggests that the compound is not rapidly metabolized in the liver (Table 1). TNP also has a decent plasma half-life (~6 h; Supplemental Figure 1R) comparable to the biguanide anti-diabetic drug metformin. Thus, TNP is bioavailable, which is also evident from our various *in vivo* studies presented in the manuscript. Plasma protein binding (PPB) of TNP is 90—93% which is similar/better than a number of FDA approved drugs [75] (Table 1). However, TNP potently inhibits human cytochrome P450s (Table 1) and thus, has a probability of causing drug—drug interactions in patients. Thus, TNP is an encouraging lead compound although it needs further structural improvement before it advances to the next level.

## 4. DISCUSSION

In summary, our study establishes that pharmacologic inhibition of the inositol pyrophosphate pathway ameliorates obesity and insulin resistance in DIO mice. TNP fails to reduce weight gain in HFD-fed IP6K1-KO mice. This result strongly suggests that the compound reduces body weight specifically via IP6K1 inhibition. Moreover, even a single-dose of TNP enhances insulin sensitivity in DIO mice by increasing Akt activity in metabolic tissues. This is consistent with our previous finding that HFD-fed IP6K1-KO mice maintain insulin sensitivity due to increased Akt activity [32]. In addition, the current study demonstrates that TNP reduces body weight, at least in part, by augmenting adipose tissue browning/thermogenesis mediated EE (Figure 7).

A coordinated increase in insulin sensitivity and EE is the ideal approach to treat obesity and T2D. Enhanced BAT mass and/or browning of WAT increases EE, which ameliorates obesity and insulin resistance in rodents [51,76,77]. Recent studies have demonstrated that humans also contain active BAT [73]. Accordingly, targeting adipose tissue thermogenesis mediated EE is an attractive anti-obesity and anti-diabetic approach [12,70,78—82]. The mechanism by which IP6K1 regulates adipose tissue browning mediated EE is not clear, although several possibilities exist. IP6K/5-IP7 inhibits Akt and LKB1-AMPK pathways whereas it stimulates CK2 (casein kinase) [34,56,83,84]. Akt and LKB1-AMPK enhance UCP1 mediated thermogenesis whereas CK2 inhibits the process [40,85—89]. Thus, IP6K1 mediated regulation of one/more of these pathways may regulate adipose tissue EE. Moreover, TNP's effects are partly albeit not entirely abolished at thermoneutral temperature, which indicates involvement of thermogenesis independent EE. The AMPK-PGC1α pathway regulates both thermogenesis dependent and independent EE [90]. TNP enhances AMPK-PGC1α signaling in cardiomyocytes [56]. PGC1α expression is also upregulated in TNP-treated adipose tissue (current study). Thus, the AMPK-PGC1α pathway seems to be one of the potentially interesting IP6K/TNP targets in EE.

What could be potential side effects of IP6K1 inhibition in obesity/T2D? A primary concern is hypoinsulinemia as IP6K1/5-IP7 promotes insulin secretion [33]. Accordingly, chow-fed IP6K1-KO mice display reduced serum insulin level [59] and are protected against HFD-induced hyperinsulinemia [32]. Moreover, TNP reduces insulin secretion from MIN6 cells [54]. The current study demonstrates that both acute and chronic TNP treatment enhances insulin sensitivity and reduces serum insulin levels in DIO WT mice to a level, which is higher/similar, but not less than CD-WT insulin level (Figures 3N and 4L). However, acute TNP does not alter serum insulin levels and its signaling in lean mice (Figure 4L, Supplemental Figure 3A and B). Short-term TNP also does not exert any effect on serum insulin level, although it enhances insulin sensitivity (Supplemental Figure 2F). In contrast to acute and long-term studies, short-term vehicle-mice do not display a HFD-induced increase in serum insulin levels, which presumably is the reason for TNP's ineffectiveness under this condition. Nevertheless, these results suggest that TNP does not cause hypoinsulinemia, it reduces HFD-induced hyperinsulinemia. The other major concern is sterility as IP6K1-KO males are sterile [59]. The current study indicates that TNP does not cause male sterility (results 3.7). There are several potential reasons as to why pharmacology does not resemble genetic deletion; i) germ-line deletion of IP6K1 may developmentally affect testes, which is not the case with TNP; ii) similar to BBB, the blood-testes barrier (BTB) blocks entry of drugs in the apical compartment [91] which presumably blocks TNP's entry. IP6K1-KO mice display social behavior

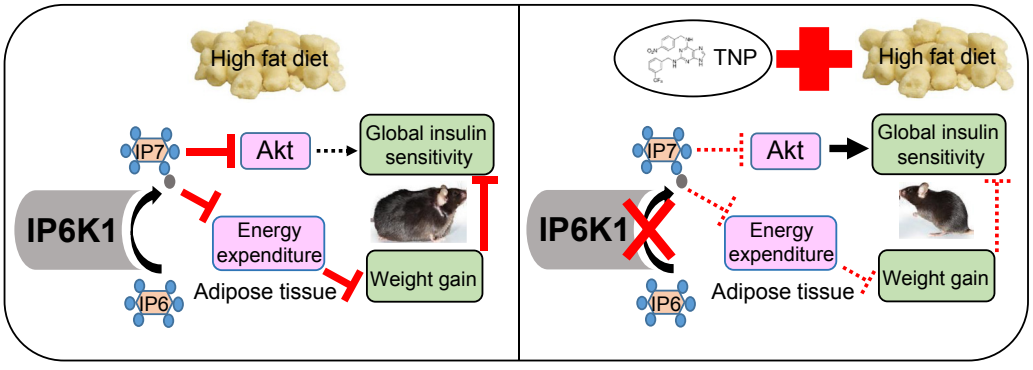


**Figure 7: Model** — IP6K1 generated 5-IP7 promotes insulin resistance in DIO mice by inhibiting the insulin sensitizing protein kinase Akt. Moreover, IP6K1 inhibits energy expenditure, in part, by modulating adipose tissue browning and thermogenesis. Accordingly, the pan IP6K inhibitor TNP ameliorates obesity and insulin resistance in DIO mice.

 © 2016 The Author(s). Published by Elsevier GmbH. This is an open access article under the CC BY-NC-ND license (http://creativecommons.org/licenses/by-nc-nd/4.0/).

deficit which could also be a potential concern in drug development [30]. Encouragingly, TNP does not efficiently cross the BBB (Supplemental Figure 1S) and thus, even its long-term treatment does not significantly alter neuronal density in the CA1 hippocampal region (Supplemental Figure 5H). TNP inhibits other IP6K isoforms which display distinct cellular functions [19,92]. TNP also exhibits certain off-target effects. For example, the compound inhibits human cytochrome P450s (Table 1) and thus, has a probability of causing drug—drug interactions in patients. Moreover, TNP slightly elevates $Ca^{2+}$ levels in human promyelocytic leukemia (HL60) cells [53] and cytosolic $Zn^{2+}$ levels in cortical neurons [93]. At higher concentrations (20—40 μM), TNP inhibits IP3-3K which enhances neurite outgrowth in PC12 cells [94]. Interestingly, TNP enhances the stimulatory phosphorylation of the extracellular signal regulated kinase (ERK) in PC12 cells [94] whereas it inhibits the same in the endothelial cells [95]. IP6K1 does not influence ERK signaling in MEF [32]; thus, the paradoxical effects of TNP on ERK signaling seem to be IP3-3K dependent. Therefore, a potent and IP6K1 specific TNP-analog is ideal to treat metabolic diseases. Alternatively, novel IP6K1 inhibitors should be developed.

TNP's long-term effects on the DIO (60% Kcals from fat) model strongly suggest that the inositol pyrophosphate pathway can be targeted in relatively less extreme human obesity. Although, life style modification is the most essential part of weight management, their long-term effects are often disappointing [3]. Therefore, a combination of drug and lifestyle intervention is ideal in these diseases [3—8]. In this regard, one of our studies indicates that mildly DIO (1-month HFD-fed) mice, when switched to chow-diet in presence of TNP, restore insulin sensitivity faster than corresponding vehicle-group (Chakraborty lab, unpublished observation). Altogether, we expect that our discovery has therapeutic relevance in obese/T2D human subjects. However, information regarding impacts of IP6K1/inositol pyrophosphates in human obesity and other related diseases is inadequate. Limited current approaches have been taken in this regard which seems to have provided promising clues [37]. Conversely, disruption of IP6K1 gene at intron 1 is observed in a single Japanese family with T2D [96]. However, the correlation does not stand with the 405 unrelated T2D patients, and thus i) is specific to the particular family or ii) is a chance association [96]. Overall, this information is insufficient and warrants further studies in humans. In conclusion, the current study hopes to incite enthusiasm for exploring the possibility of pharmacologic inhibition of the inositol pyrophosphate pathway in human obesity, T2D, and other relevant diseases.

## FUNDING

The work is supported by R01DK103746 and TSRI startup fund 1-31564 to Anutosh Chakraborty. Baoji Xu is supported by DK103335.

## AUTHOR CONTRIBUTIONS

A.C. conceptualized the project; A.C., S.G., Q.Z., M.C., B.X. and T.K. designed experiments; T.K., H.L. and A.A. synthesized TNP; J.C.B and G.E provided a separate batch of TNP; S.G., Q.Z., H.X. and M.C. performed experiments; A.C., S.G., Q.Z., T.K. B.X. and M.C. analyzed data; A.C. wrote the paper.

## ACKNOWLEDGEMENTS

We sincerely thank the Snyder lab for providing IP6K1-KO mice, [3H]IP6 and various other reagents; Ugander Gajjalaiahvari and Biki Bapi Kundu for their experimental assistance in IP6K1 activity assays; Roy Smith and Andras Kern for sharing QPCR probes and The TSRI M&A department for sharing instruments and reagents.

## CONFLICT OF INTEREST

None.

## APPENDIX A. SUPPLEMENTARY DATA

Supplementary data related to this article can be found at http://dx.doi.org/10.1016/j.molmet.2016.08.008.

## REFERENCES

[1] Kahn, B.B., Kahn, F.J., 2000. Obesity and insulin resistance. Journal of Clinical Investigation 106:473—481.
[2] Hardy, O.T., C.M., Corvera, S., 2012. What causes the insulin resistance underlying obesity? Current Opinion in Endocrinology Diabetes and Obesity 19:81—87.
[3] Hainer, V., H.I., 2012. Do we need anti-obesity drugs? Diabetes/Metabolism Research and Reviews 28:8—20.
[4] Kim, G.W., L.J., Blomain, E.S., Waldman, S.A., 2014. Antiobesity pharmacotherapy: new drugs and emerging targets. Clinical Pharmacology & Therapeutics 95:53—66.
[5] Rodgers, R.J., T.M., Wilding, J.P., 2012. Anti-obesity drugs: past, present and future. Disease Models & Mechanisms 5:621—626.
[6] Vervoort, G., T.C., 2007. Do we need new drugs for the treatment of type 2 diabetes mellitus? Netherlands Journal of Medicine 65:157—159.
[7] Yanovski, S.Z., Y.J., 2014. Long-term drug treatment for obesity: a systematic and clinical review. JAMA 311:74—86.
[8] Witkamp, R.F., 2011. Current and future drug targets in weight management. Pharmaceutical Research 28:1792—1818.
[9] Holes-Lewis, K.A., M.R., O'Neil, P.M., 2013. Pharmacotherapy of obesity: clinical treatments and considerations. American Journal of the Medical Sciences 345:284—288.
[10] Whittle, A., R.-P.J., Vidal-Puig, A., 2013. Pharmacological strategies for targeting BAT thermogenesis. Trends in Pharmacological Sciences 34:347—355.
[11] Rondinone, C., 2005. Serine kinases as new drug targets for the treatment of type 2 diabetes. Current medicinal chemistry-immunology. Endocrine & Metabolic Agents 5:529—536.
[12] Tseng, Y.H., C.A., Kahn, C.R., 2010. Cellular bioenergetics as a target for obesity therapy. Nature Reviews Drug Discovery 9:465—482.
[13] Choi, J.H., B.A., Estall, J.L., Kajimura, S., Boström, P., Laznik, D., et al., 2010. Anti-diabetic drugs inhibit obesity-linked phosphorylation of PPARgamma by Cdk5. Nature 466:451—456.
[14] Hansen, J.B., A.P., Bodvarsdottir, T.B., Wahl, P., 2004. Inhibition of insulin secretion as a new drug target in the treatment of metabolic disorders. Current Medicinal Chemistry 11:1595—1615.
[15] Nilsson, C., R.K., Yan, F.F., Larsen, M.O., Tang-Christensen, M., 2012. Laboratory animals as surrogate models of human obesity. Acta Pharmacologica Sinica 33:173—181.
[16] Collins, S., M.T., Surwit, R.S., Robidoux, J., 2004. Genetic vulnerability to diet-induced obesity in the C57BL/6J mouse: physiological and molecular characteristics. Physiology & Behavior 81:243—248.
[17] Buettner, R., S.J., Bollheimer, L.C., 2007. High-fat diets: modeling the metabolic disorders of human obesity in rodents. Obesity (Silver Spring) 15:798—808.
[18] Cohen, P., A.D., 2013. Kinase drug discovery—what's next in the field? ACS Chemical Biology 8:96—104.
[19] Chakraborty, A., K.S., Snyder, S.H., 2011. Inositol pyrophosphates as mammalian cell signals. Science Signalling 4:re1.

 © 2016 The Author(s). Published by Elsevier GmbH. This is an open access article under the CC BY-NC-ND license (http://creativecommons.org/licenses/by-nc-nd/4.0/). 

[20] Wilson, M.S., L.T., Saiardi, A., 2013. Inositol pyrophosphates: between signalling and metabolism. Biochemical Journal 452:369—379.
[21] Thota, S.G., B.R., 2015. The emerging roles of inositol pyrophosphates in eukaryotic cell physiology. Journal of Biosciences 40:593—605.
[22] Shears, S., 2016. Towards pharmacological intervention in inositol pyrophosphate signalling. Biochemical Society Transactions 44:191—196.
[23] Barker, C.J., I.C., Gaboardi, G.C., Berggren, P.O., 2009. Inositol pyrophosphates: structure, enzymology and function. Cellular and Molecular Life Sciences 66:3851—3871.
[24] Saiardi, A., E.-B.H., Snowman, A.M., Tempst, P., Snyder, S.H., 1999. Synthesis of diphosphoinositol pentakisphosphate by a newly identified family of higher inositol polyphosphate kinases. Current Biology 9:1323—1326.
[25] Saiardi, A., N.E., Luo, H.R., Snowman, A.M., Snyder, S.H., 2001. Identification and characterization of a novel inositol hexakisphosphate kinase. Journal of Biological Chemistry 276:39179—39185.
[26] Wundenberg, T., G.N., Lin, H., Mayr, G.W., 2014. Discovery of InsP6-kinases as InsP6-dephosphorylating enzymes provides a new mechanism of cytosolic InsP6 degradation driven by the cellular ATP/ADP ratio. Biochemical Journal 462:173—184.
[27] Chanduri, M., R.A., Malla, A.B., Wu, M., Fiedler, D., Mallik, R., et al., 2016. Inositol hexakisphosphate kinase 1 (IP6K1) activity is required for cytoplasmic dynein-driven transport. Biochemical Journal p. pii: BCJ20160610.
[28] Ghosh, S., S.D., Suman, K., Lakshmi, B.J., Manorama, R., Kumar, S., et al., 2013. Inositol hexakisphosphate kinase 1 maintains hemostasis in mice by regulating platelet polyphosphate levels. Blood 122:1478—1486.
[29] Ghoshal, S., T.R., Zhu, Q., Chakraborty, A., 2016 Jun 29. Inositol hexakisphosphate kinase-1 interacts with perilipin1 to modulate lipolysis. International Journal of Biochemistry & Cell Biology 78:149—155.
[30] Chakraborty, A., L.C., Xu, J., Snyder, S.H., Beaulieu, J.M., 2014. Inositol hexakisphosphate kinase-1 regulates behavioral responses via GSK3 signaling pathways. Molecular Psychiatry 19:284—293.
[31] Luo, H.R., S.A., Nagata, E., Ye, K., Yu, H., Jung, T.S., et al., 2001. GRAB: a physiologic guanine nucleotide exchange factor for Rab3A, which interacts with inositol hexakisphosphate kinase. Neuron 31:439—451.
[32] Chakraborty, A., K.M., Bello, N.T., Maxwell, M., Potter, J.J., Juluri, K.R., et al., 2010. Inositol pyrophosphates inhibit Akt signaling, regulate insulin sensitivity and weight gain. Cell 143:897—910.
[33] Illies, C., G.J., Fiume, R., Leibiger, B., Yu, J., Juhl, K., et al., 2007. Requirement of inositol pyrophosphates for full exocytotic capacity in pancreatic beta cells. Science 318:1299—1302.
[34] Szijgyarto, Z., G.A., Azevedo, C., Saiardi, A., 2011. Influence of inositol pyrophosphates on cellular energy dynamics. Science 334:802—805.
[35] Manning, B.D., C.L., 2007. AKT/PKB signaling: navigating downstream. Cell 129:1261—1274.
[36] Summers, S.A., B.M., 1997. A role for the serine/threonine kinase, Akt, in insulin-stimulated glucose uptake. Biochemical Society Transactions 25:981—988.
[37] Mackenzie, R.W., E.B., 2014. Akt/PKB activation and insulin signaling: a novel insulin signaling pathway in the treatment of type 2 diabetes. Diabetes, Metabolic Syndrome and Obesity: Targets and Therapy 13:55—64.
[38] Cho, H., M.J., Kim, J.K., Thorvaldsen, J.L., Chu, Q., Crenshaw 3rd, E.B., et al., 2001. Insulin resistance and a diabetes mellitus-like syndrome in mice lacking the protein kinase Akt2 (PKB beta). Science 292:1728—1731.
[39] Izumiya, Y., H.T., Morris, C., Sato, K., Zeng, L., Viereck, J., et al., 2008. Fast/Glycolytic muscle fiber growth reduces fat mass and improves metabolic parameters in obese mice. Cell Metabolism 7:159—172.
[40] Hui, X., G.P., Zhang, J., Nie, T., Pan, Y., Wu, D., et al., 2015. Adiponectin enhances cold-induced browning of subcutaneous adipose tissue via promoting M2 macrophage proliferation. Cell Metabolism 22:279—290.
[41] Karlsson, H.K., Z.J., Kane, S., Krook, A., Lienhard, G.E., Wallberg-Henriksson, H., 2005. Insulin-stimulated phosphorylation of the Akt substrate AS160 is impaired in skeletal muscle of type 2 diabetic subjects. Diabetes 54:1692—1697.
[42] Krook, A., R.R., Jiang, X.J., Zierath, J.R., Wallberg-Henriksson, H., 1998. Insulin-stimulated Akt kinase activity is reduced in skeletal muscle from NIDDM subjects. Diabetes 47:1281—1286.
[43] Jordan, S.D., K.M., Willmes, D.M., Redemann, N., Wunderlich, F.T., Brönneke, H.S., et al., 2011. Obesity-induced overexpression of miRNA-143 inhibits insulin-stimulated AKT activation and impairs glucose metabolism. Nature Cell Biology 13:434—446.
[44] Farese, R.V., S.M., Standaert, M.L., 2005. Insulin-sensitive protein kinases (atypical protein kinase C and protein kinase B/Akt): actions and defects in obesity and type II diabetes. Experimental Biology and Medicine (Maywood) 230:593—605.
[45] Prasad, A., J.Y., Chakraborty, A., Li, Y., Jain, S.K., Zhong, J., et al., 2011. Inositol hexakisphosphate kinase 1 regulates neutrophil function in innate immunity by inhibiting phosphatidylinositol-(3,4,5)-trisphosphate signaling. Nature Immunology 12:752—760.
[46] Xu, Y., L.H., Bajrami, B., Kwak, H., Cao, S., Liu, P., et al., 2013. Cigarette smoke (CS) and nicotine delay neutrophil spontaneous death via suppressing production of diphosphoinositol pentakisphosphate. Proceedings of the National Academy of Sciences of the United States of America 110:7726—7731.
[47] Luo, H.R., H.Y., Chen, J.C., Saiardi, A., Iijima, M., Ye, K., et al., 2003. Inositol pyrophosphates mediate chemotaxis in Dictyostelium via pleckstrin homology domain-PtdIns(3,4,5)P3 interactions. Cell 114:559—572.
[48] Wu, M., D.B., Trevisan, A.J., Fiedler, D., 2013. Synthesis and characterization of non-hydrolysable diphosphoinositol polyphosphate second messengers. Chemical Science 4:405—410.
[49] Pavlovic, I., T.D., Vargas, J.R., McKinlay, C.J., Hauke, S., Anstaett, P., et al., 2016. Cellular delivery and photochemical release of a caged inositol-pyrophosphate induces PH-domain translocation in cellulo. Nature Communications 7:10622.
[50] Rosen, E.D., S.B., 2014. What we talk about when we talk about fat. Cell 156:20—44.
[51] Harms, M., S.P., 2013. Brown and beige fat: development, function and therapeutic potential. Nature Medicine 19:1252—1263.
[52] N, T.G.a.M, 2006. In: Mantovani, G. (Ed.), Diet-induced thermogenesis. Springer, 4.
[53] Chang, Y.T., C.G., Bae, Y.S., Burdett, M., Moon, H.S., Lee, J.W., et al., 2002. Purine-based inhibitors of inositol-1,4,5-trisphosphate-3-kinase. ChemBioChem 3:897—901.
[54] Padmanabhan, U., D.D., Fridy, P.C., York, J.D., Downes, C.P., 2009. Characterization of a selective inhibitor of inositol hexakisphosphate kinases: use in defining biological roles and metabolic relationships of inositol pyrophosphates. Journal of Biological Chemistry 284:10571—10582.
[55] Wang, H., F.J., Hall, T.M., Shears, S.B., 2011. Structural basis for an inositol pyrophosphate kinase surmounting phosphate crowding. Nature Chemical Biology 8:111—116.
[56] Sun, D., L.S., Wu, H., Zhang, M., Zhang, X., Wei, L., et al., 2015. (OSM) protects against cardiac ischaemia/reperfusion injury in diabetic mice by regulating apoptosis, mitochondrial biogenesis and insulin sensitivity. Journal of Cellular and Molecular Medicine 19:1296—1307.
[57] Zhang, Z., Z.C., Liu, B., Liang, D., Qin, X., Li, X., et al., 2014. Inositol pyrophosphates mediate the effects of aging on bone marrow mesenchymal stem cells by inhibiting Akt signaling. Journal of Stem Cell Research & Therapy 5:33.
[58] Sarmah, B., W.S., 2010. Inositol hexakisphosphate kinase-2 acts as an effector of the vertebrate Hedgehog pathway. Proceedings of the National Academy of Sciences of the United States of America 107:19921—19926.
[59] Bhandari, R., J.K., Resnick, A.C., Snyder, S.H., 2008. Gene deletion of inositol hexakisphosphate kinase 1 reveals inositol pyrophosphate regulation of insulin

 © 2016 The Author(s). Published by Elsevier GmbH. This is an open access article under the CC BY-NC-ND license (http://creativecommons.org/licenses/by-nc-nd/4.0/).

secretion, growth, and spermiogenesis. Proceedings of the National Academy of Sciences of the United States of America 105:2349–2353.
[60] Chakraborty, A., K.M., Sixt, K.M., Juluri, K.R., Mustafa, A.K., Snowman, A.M., et al., 2008. HSP90 regulates cell survival via inositol hexakisphosphate kinase-2. Proceedings of the National Academy of Sciences of the United States of America 105:1134–1139.
[61] Losito, O., S.Z., Resnick, A.C., Saiardi, A., 2009. Inositol pyrophosphates and their unique metabolic complexity: analysis by gel electrophoresis. PLoS One 4:e5580.
[62] Tschöp, M.H., S.J., Arch, J.R., Auwerx, J., Brüning, J.C., Chan, L., et al., 2011. A guide to analysis of mouse energy metabolism. Nature Methods 9:57–63.
[63] Baydyuk, M., X.Y., Tessarollo, L., Xu, B., 2013. Midbrain-derived neurotrophins support survival of immature striatal projection neurons. Journal of Neuroscience 33:3363–3369.
[64] Regeur, L., P.B., 1989. Optimizing sampling designs for volume measurements of components of human brain using a stereological method. Journal of Microscopy 155:113–121.
[65] Henninger, D.D., G.M., Granger, D.N., 1997. Low-density lipoprotein receptor knockout mice exhibit exaggerated microvascular responses to inflammatory stimuli. Circulation Research 81:274–281.
[66] Sarbassov, D.D., G.D., Ali, S.M., Sabatini, D.M., 2005. Phosphorylation and regulation of Akt/PKB by the rictor-mTOR complex. Science 307:1098–1101.
[67] Alessi, D.R., J.S., Downes, C.P., Holmes, A.B., Gaffney, P.R., Reese, C.B., et al., 1997. Characterization of a 3-phosphoinositide-dependent protein kinase which phosphorylates and activates protein kinase Balpha. Current Biology 7:261–269.
[68] Rothwell, N.J., S.M., 1997. A role for brown adipose tissue in diet-induced thermogenesis. Obesity Research 5:650–656.
[69] Kozak, L.P., A.-K.R, 2008. UCP1: its involvement and utility in obesity. International Journal of Obesity (Lond) 32(Suppl. 7):S32–S38.
[70] Chechi, K., N.J., Richard, D., 2013. Brown adipose tissue as an anti-obesity tissue in humans. Obesity Review.
[71] Bachman, E.S., D.H., Zhang, C.Y., Cinti, S., Bianco, A.C., Kobilka, B.K., et al., 2002. betaAR signaling required for diet-induced thermogenesis and obesity resistance. Science 297:843–845.
[72] Gimeno, R.E., M.D., 2014. FGF21-based pharmacotherapy—potential utility for metabolic disorders. Trends in Endocrinology and Metabolism 25:303–311.
[73] Cypess, A.M., W.L., Roberts-Toler, C., Franquet Elía, E., Kessler, S.H., Kahn, P.A., et al., 2015. Activation of human brown adipose tissue by a β3-adrenergic receptor agonist. Cell Metabolism 21:33–38.
[74] Collins, S., 2014. A heart-adipose tissue connection in the regulation of energy metabolism. Nature Reviews Endocrinology 10:157–163.
[75] Smith, D.A., D.L., Kerns, E.H., 2010. The effect of plasma protein binding on in vivo efficacy: misconceptions in drug discovery. Nature Reviews Drug Discovery 9:929–939.
[76] Bi, P., S.T., Liu, W., Yue, F., Yang, X., Liang, X.R., et al., 2014. Inhibition of Notch signaling promotes browning of white adipose tissue and ameliorates obesity. Nature Medicine.
[77] Boström, P., W.J., Jedrychowski, M.P., Korde, A., Ye, L., Lo, J.C., et al., 2012. A PGC1-α-dependent myokine that drives brown-fat-like development of white fat and thermogenesis. Nature 481:463–468.
[78] Pilch, P.F., B.N., 2006. Pharmacological targeting of adipocytes/fat metabolism for treatment of obesity and diabetes. Molecular Pharmacology 70:779–785.
[79] Cypess, A.M., K.C., 2010. Brown fat as a therapy for obesity and diabetes. Current Opinion in Endocrinology Diabetes and Obesity 17:143–149.
[80] Cypess, A.M., L.S., Williams, G., Tal, I., Rodman, D., Goldfine, A.B., et al., 2009. Identification and importance of brown adipose tissue in adult humans. New England Journal of Medicine 360:1509–1517.
[81] Müller, M.J., B.-W.A., 2013. Adaptive thermogenesis with weight loss in humans. Obesity (Silver Spring) 21:218–228.
[82] Yoneshiro, T., A.S., Matsushita, M., Kayahara, T., Kameya, T., Kawai, Y., et al., 2013. Recruited brown adipose tissue as an antiobesity agent in humans. Journal of Clinical Investigation 123:3404–3408.
[83] Rao, F., X.J., Fu, C., Cha, J.Y., Gadalla, M.M., Xu, R., et al., 2015. Inositol pyrophosphates promote tumor growth and metastasis by antagonizing liver kinase B1. Proceedings of the National Academy of Sciences of the United States of America.
[84] Rao, F., C.J., Xu, J., Xu, R., Vandiver, M.S., Tyagi, R., et al., 2014. Inositol pyrophosphates mediate the DNA-PK/ATM-p53 cell death pathway by regulating CK2 phosphorylation of Tti1/Tel2. Molecular Cell 54:119–132.
[85] Hinoi, E., I.T., Fujita, H., Watanabe, T., Odaka, Y., Ozaki, K., et al., 2014. PI3K/Akt is involved in brown adipogenesis mediated by growth differentiation factor-5 in association with activation of the Smad pathway. Biochemical and Biophysical Research 450:255–260.
[86] Valverde, A.M., A.M., Mur, C., Navarro, P., Pons, S., Cassard-Doulcier, A.M., et al., 2003. Insulin-induced up-regulated uncoupling protein-1 expression is mediated by insulin receptor substrate 1 through the phosphatidylinositol 3-kinase/Akt signaling pathway in fetal brown adipocytes. Journal of Biological Chemistry 278:10221–10231.
[87] Zhang, H., G.M., Townsend, K.L., Huang, T.L., An, D., Yan, X., et al., 2015. MicroRNA-455 regulates brown adipogenesis via a novel HIF1an-AMPK-PGC1α signaling network. EMBO Reports 16:1378–1393.
[88] van Dam, A.D., K.S., Schilperoort, M., Rensen, P.C., Boon, M.R., 2015. Regulation of brown fat by AMP-activated protein kinase. Trends in Molecular Medicine. S1471–4914(15)00136-7.
[89] Shinoda, K., O.K., Hasegawa, Y., Chang, H.Y., Ogura, M., Sato, A., et al., 2015. Phosphoproteomics identifies CK2 as a negative regulator of beige adipocyte thermogenesis and energy expenditure. Cell Metabolism 22:997–1008.
[90] Cantó, C., A.J., 2009. PGC-1alpha, SIRT1 and AMPK, an energy sensing network that controls energy expenditure. Current Opinion in Lipidology 20:98–105.
[91] Cheng, C.Y., M.D., 2012. The blood-testis barrier and its implications for male contraception. Pharmacological Reviews 64:16–64.
[92] Fu, C., X.J., Li, R.J., Crawford, J.A., Khan, A.B., Ma, T.M., et al., 2015. Inositol hexakisphosphate Kinase-3 regulates the morphology and synapse formation of cerebellar purkinje cells via spectrin/adducin. Journal of Neuroscience 35:11056–11067.
[93] Stork, C.J., L.Y., 2010. Zinc release from thapsigargin/IP3-sensitive stores in cultured cortical neurons. Journal of Molecular Signaling 5:5.
[94] Eva, R., B.-C.D., Patel, K., Cullen, P.J., Banting, G., 2012. IP3 3-kinase opposes NGF driven neurite outgrowth. PLoS One 7:e32386.
[95] Sekar, M.C., S.K., Leloup, L., Wells, A., 2014. Modulation of epidermal growth factor stimulated ERK phosphorylation and cell motility by inositol trisphosphate kinase. Journal of Pharmaceutical Sciences and Pharmacology 1:160–164.
[96] Kamimura, J., W.K., Kadowaki, H., Watanabe, Y., Miyake, K., Harada, N., et al., 2004. The IHPK1 gene is disrupted at the 3p21.31 breakpoint of t(3;9) in a family with type 2 diabetes mellitus. Journal of Human Genetics 49:360–365.

 © 2016 The Author(s). Published by Elsevier GmbH. This is an open access article under the CC BY-NC-ND license (http://creativecommons.org/licenses/by-nc-nd/4.0/). 